Arabian Journal of Chemistry (2022) **15**, 103986

King Saud University

Arabian Journal of Chemistry

www.ksu.edu.sa
www.sciencedirect.com

ORIGINAL ARTICLE

Cytotoxic urea Schiff base complexes for multidrug discovery as anticancer activity and low *in vivo* oral assessing toxicity

Lotfi M. Aroua [a,b,c,*], **Ahmed N. Al-Hakimi** [a,d], **Mahfoudh A.M. Abdulghani** [e], **Sadeq K. Alhag** [f]

[a] *Department of Chemistry, College of Science, Qassim University, Campus University, King Abdulaziz Road, Al-Malida, 51452 - P. O.Box: 6644, Buraydah, Qassim, Saudi Arabia*
[b] *Laboratory of Organic Structural Chemistry and Macromolecules, Department of Chemistry, Faculty of Sciences of Tunis, Tunis El-Manar University, El Manar I 2092, Tunis, Tunisia*
[c] *Carthage University, Department of Chemistry, Faculty of Sciences of Bizerte, 7021 Jarzouna, Tunisia*
[d] *Department of Chemistry, Faculty of Sciences, Ibb University, Ibb, Yemen*
[e] *Department of Pharmacology & Toxicology, Unaizah College of Pharmacy, Qassim University, 5919 Qassim, Saudi Arabia*
[f] *Biology Department, College of Science and Arts, King Khalid University, Muhayl Asser, Saudi Arabia*

Received 25 March 2022; accepted 19 May 2022
Available online 27 May 2022

KEYWORDS

Anticancer activity;
Complex;
Urea;
Schiff base;
Low *in vivo* assessing toxicity

Abstract Novel mononuclear complexes **2**–**8** derived from hybrid Urea Schiff base **HL** were synthesized using various metal Ni^{2+}, Fe^{3+}, Cu^{2+}, Co^{2+}, Mn^{2+}, Zn^{2+}, and Cr^{3+}. The results revealed the ligand **HL** reacts with metal ions as monobasic or neutral monodentate chelator it via the nitrogen of azomethine and deprotonated/protonated phenolic oxygen atom adopting octahedral geometry. The elemental analysis of the complexes showed the bonding of the ligand with the metal ions in a ratio of 1: 1 in all-metal complexes. XRD analysis of the ligand and its complexes indicate a monoclinic, tetragonal, orthorhombic corresponding to urea Shiff base **(1)** and zinc complex **(7),** nickel complex **(2)**, and cobalt complexes **(5),** respectively. The bioactivity of synthesized compounds was tested and screened against three cancer cell lines **PC3** (prostate), **SK-OV-3** (ovarian), and **HeLa** (cervical). The results revealed a weak activity for the ligand, whereas nickel and iron complexes present moderate activities against three cancer cells. The best results were mentioned with copper and proved the best results against three cancer cells **PC3**, **SKOV3,** and **HeLa** displaying an excellent activity with IC_{50} values of **0.71 ± 0.06**, **0.12 ± 0.06,** and **0.79 ± 0.23** μg/mL respectively. Moreover, the urea Schiff base complexes showed good safety *in vivo* toxicity test.

* Corresponding author.
E-mail address: lm.aroua@qu.edu.sa (L.M. Aroua).
Peer review under responsibility of King Saud University.

Production and hosting by Elsevier

https://doi.org/10.1016/j.arabjc.2022.103986

The present study demonstrates that all urea Schiff base complexes is inactive against saint tissue and five metal complexes investigated herein can be effective and promising chemotherapeutic drugs for ovarian cancer cell SKOV3, emphasizing the copper-urea Schiff base complex.

1. Introduction

Cancer is a challenging disease worldwide due to several reasons. Firstly, cancer is a commonly fatal disease that causes a very high incidence and mortality rate globally. According to the world health organization, cancer disease caused 9.6 million deaths in 2018. One out of six deaths was due to cancer in many countries, with an estimated 20 million deaths for 2030 (Hanusova et al., 2015; Yadav et al., 2016). Secondly, cancer can affect various organs of different systems of the body in both gender male and female. Cancer can progress at different stages, and each type needs treatment (Martínez-Jiménez et al., 2020; Lee et al., 2020; Bose et al., 2020). In males, prostate cancer is the second most common malignancy globally and has a high mortality rate, causing 1.3 million deaths in 2018. Several gynecological cancers, including ovarian, cervical, and endometrial, have been reported as life-threatening diseases in women (Tam et al., 2021). Ovarian cancer is one of the most dangerous gynecologic cancers that extremely menace women's health (Younes et al., 2019). Usually, ovarian cancer is diagnosed at stage 3 or 4, resulting in a 5-year survival rate of 30% over the past 30 years (Younes et al., 2019). More than 600,000 new cases in women with cervical cancer and more than 340,000 cervical cancer deaths worldwide in 2020 (Sung et al., 2021, Crosbie et al, 2013, Di et al, 2015). Endometrial cancer represents the most common gynecological malignancy in the western world (Chaudhry and Asselin, 2009).

Finally, chemoresistance in cancers is a severe treatment challenge, especially in reproductive cancers. Cancer chemotherapy is one of the major therapeutic approaches for treating the disease, which may be used alone or combined with other forms of therapy. Drug resistance is a major obstacle in treating ovarian cancer (Li et al., 2000). The development of resistance to agents used in cancer treatment is a major obstacle to the successful abolishment of the disease (Mihanfar et al., 2017). The response rate of cancer to cytotoxic agents has not reached acceptable levels. The development of chemotherapy resistance continues to be the main problem in the treatment of cancer patients. Moreover, the cancer cells' resistance and dose-related toxicity remain two of the utmost significant limitations in cancer chemotherapy.

There is a need for novel agents that are effective in drug-resistant cancers. The necessity to design and elaborate a novel structure promising anticancer activities encouraged scientists to discover new agents. Therefore, new chemotherapeutic agents for cancer might improve the response of cancer cells and overcome these drawbacks. Finding a new drug has pointed researchers to think about new agents with lower systemic toxicity and enhanced cytotoxic effect.

Schiff base represents a fundamental precursor to develop diversely metal complexes having curative potential as antibacterial (Madani et al., 2020; Xu et al., 2020), antimicrobial and antiproliferative agents (Poirier et al., 2013, Savcı et al., 2021, Ahmed and Almalki, 2021), antifungal (Miloud et al., 2020; Joshi et al., 2020), antimalarial (Ziegler et al., 2000; Savir et al., 2020), anti-inflammatory (Bhuvaneswari et al., 2020), antioxidant (Bhuvaneswari et al., 2020, Buldurun et al., 2021), DNA binding (Revathi et al., 2020) and *in vivo* acute toxicity and anti-gastric (Saremi et al., 2020). Moreover, complexes elaborated from Schiff base was used currently as antitumor (Chen et al., 2020; Liu et al., 2020) and anticancer agents (Alminderej et al., 2021; Ahamad et al., 2020; Crans et al., 2019; Galil et al., 2015). A variety of structure derived from Schiff base complex was described as potent anticancer agent such as macrocycles (Zayed et al., 2017), dehydroacetic acid based hydrazine (Pal et al., 2014), hydrazine carboxamide, 2-[3-methyl-2-thienylmethylene] (Chandra et al., 2015), aroylhydrazone ligands and a pyridine co-ligand (Gou et al., 2017) and thiadiazoline moiety (Parsekar et al., 2022).

A multitude of reports described the anticancer activities of Schiff base complexes were investigated using variety of human tumour cell lines including human liver carcinoma (Hep-G2) cells (Ismail et al., 2021, Adwin et al, 2020), human breast MCF-7 (Fayed et al., 2021; Ma et al., 2012), ovarian cancer cell lines SKOV-3 (Sukanya et al., 2018; Sedighipoor et al., 2019, Alorini et al., 2022), prostate cancer cell PC3 (Parveen et al., 2020; Tabassum et al., 2013), cervical cancer cells HeLa (Ahamad et al., 2020; Andiappan et al., 2018; Das et al., 2020), adenocarcinomic human alveolar basal epithelial cells A 549 (Ali et al., 2020), human colon cancer cell line HCT-116 (Dasgupta et al., 2020) and renal cell carcinoma A498 (Garza-Ortiz et al., 2013).

Urea is a magnificent class of target organic compounds owing diversely application in different fields covering biological and coordination chemistry. Compounds derived from urea fascinate researchers to create novel structures owing multitude of biological activities and medicinal applications (Sabir et al., 2021; Faidallah et al., 2011; Kollu et al., 2021). The coordination of urea with various metal lead to multiple target metallo-scaffolds manifesting different biological activities (Mohapatra et al., 2021; Sroor et al., 2022; Lin et al., 2021). Complexes derived from urea were reviewed as potent anticancer agents in many reports (Uprety et al., 2022). Many structures of complexes involved urea moiety was investigated as anticancer candidate including *N*-heterocyclic carbene (NHC) complexes (Jakob et al., 2021), pyrimidine-pyrazoles (Cherukumalli et al., 2022), 1,4-Diisocyanatobenzene (Nagalakshmamma et al., 2021), 2-formyl tetrahydronaphthyridine (Zhang et al., 2022), thiazolyl-urea (Sroor et al., 2022) and Biotinylated curcumin (Garza-Ortiz et al., 2013).

Complexes derived from the urea nucleus frequently manifested anticancer activities toward several human cancer cell lines, including prostate cancer cell PC3 (Abdullahi et al., 2020, Aras and Yerlikaya, 2016), cervical cancer cells HeLa (Poyraz et al., 2017), human breast cancer cell MCF-7 (Banti et al., 2020), human lung cancer cell lines (NCI-H23)

(Vikram et al., 2020), human colon cancer cell line HCT116 (Xie et al., 2015), human monocytic leukemia cell line THP-1 (Asghar et al., 2017).

Many drugs introduced in the market containing urea moiety, including Sorafenib (diarylurea) was prescript in the therapy of advanced renal cell carcinoma (RCC) (Raoul et al., 2018). Linifanib (diarylurea) is used as a therapy for non-small cell lung carcinoma (NSCLC), liver cancer, breast cancer, colorectal cancer (Borriello et al., 2017). Tivozanib (diarylurea) shown considerable efficacy for the treatment of advanced RCC over the past decade (Salgia et al., 2020) (Fig. 1). In addition, several structures having aryl or diaryl Schiff base possess significant activities toward human cancer cells covering PC3, SKOV3, and HeLa (Fig. 1) (see Figs. 2-4).

As a consequence, we designed a new target scaffold ligand owing both pharmacophores diaryl urea and diaryl Schiff base in the same structure. Gathering the two patterns in one molecule and combining their properties was our purpose and presents a new way to increase the efficiency of biologically active molecules. In this work, we developed a novel molecule that combines the pharmacophores diarylurea and diaryl Schiff base. The synthesised target complexes were examined for minimal *in vivo* oral toxicity to establish their safety and approved their efficacy as anticancer medicines for multidrug regimens.

The elaboration of novel anticancer drugs capable of curing cancer diseases become a first challenge to the global healthcare system. In continuation to develop and discover new structures having biological activities (Aroua et al., 2020; Ghrab et al., 2017; Aroua et al., 2020, Ghrab et al., 2017) with low in vivo toxicity in the same molecule, a series of novel urea Schiff base complexes 2–8 were synthesized. The screening activities of cytotoxic effect on PC-3, SKOV3, HeLa cancer cell lines, and in vivo subacute toxicity were studied.

2. Experimental

2.1. General details

FT-IR spectra were achieved using Agilent FT-IR Spectrometer Cary 600 with microscope in the range of 400–4000 cm^{-1}. The ^{1}H and ^{13}C NMR spectra were recorded on a 850 MHz NMR spectrometer Bruker Avance III HD at 850 and 213 MHz, respectively. All spectra were obtained using DMSOd_6 as a solvent and referenced to TMS. Chemical shifts of ^{1}H NMR spectra are reported in parts per million (ppm) on the δ scale from an internal standard of residual DMSO (2.50 ppm). Data are reported as follows: chemical shift, integration, multiplicity (s = singlet, d = doublet, t = triplet, q = quartet, and m = multiplet) and coupling constant in hertz (Hz). Chemical shifts of ^{13}C NMR spectra are reported in ppm from the central peak of DMSOd_6 (39.52 ppm) on the δ scale. The elemental analysis was carried out on Flash *Smart* Elemental Analyzer Thermo Fisher Scientific performing carbon, hydrogen and nitogen (CHN) analyses.

The melting points were measured in open capillary tubes using The Stuart SMP30 Apparatus. Analytical TLC was performed using Silica Gel 60 F254 plates (Sigma 40–60 μm). The developed chromatogram was visualized under UV lamp (254 nm). All commercially available reagents were purchased from Sigma-Aldrich and used without further purification. Absolute ethanol was used as solvent. All reactions were carried using oven-dried glassware unless otherwise stated.

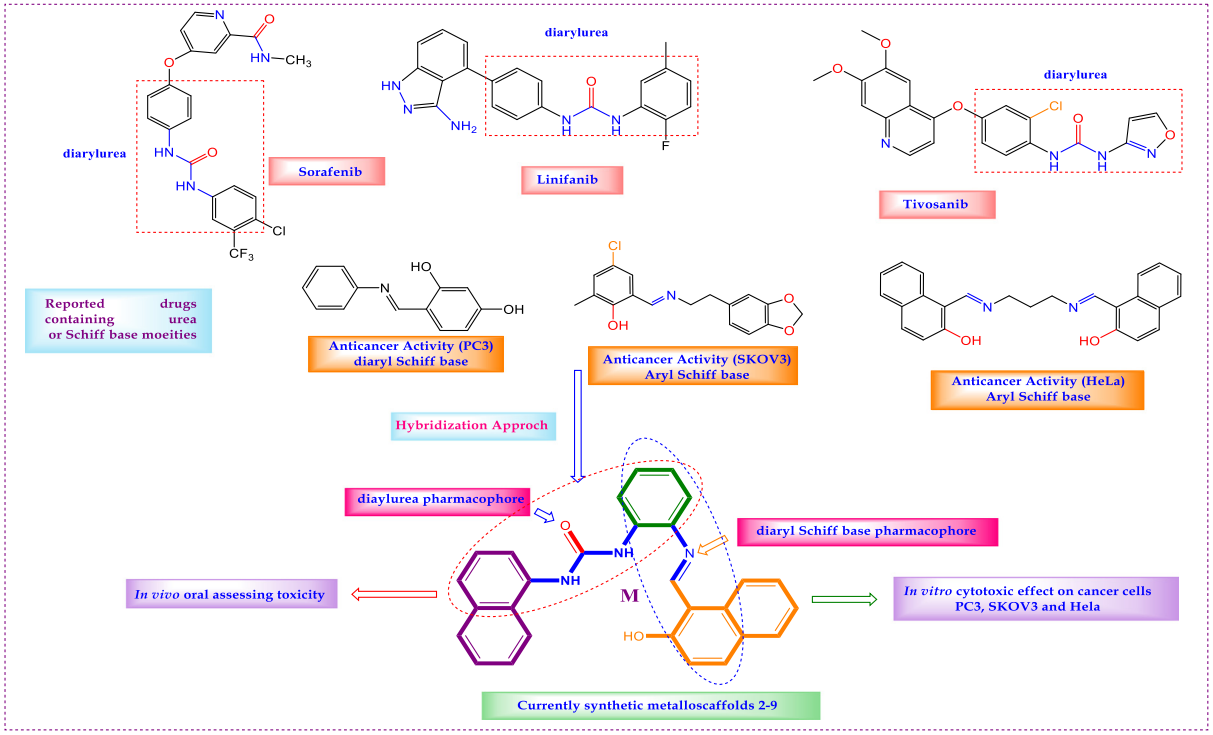

Fig. 1 Design of novel Urea bridged with Schiff base hybrids.

2.2. Chemistry

2.2.1. General procedure for synthesis of (2-aminophenyl)-3-(naphthalen-1-yl)urea (3′)

1.08 g (10 mmol) of *o*-phenylenediamine in 15 mL of dichloromethane was added to a solution containing 10 mmol of naphthyl isocyanate in 40 mL of dichloromethane. The mixture was stirred at room temperature for 30 mn. The reaction progress was monitored by TLC using diethyl ether/hexane (70/30) as eluent. The reaction mixture was filtered and the crude solid was purified by recrystallization from ethanol.

White precipitate, yield: 90%; M.p. 280–282 °C; IR (cm^{-1}) *v*: 3258 (NH), 1646 (C = O), 1606 (C = N); 1547 (C = C);^{1}H NMR (850 MHz, DMSO d_6) δ(ppm): 8.85 (s, 1H, NH), 8.21–8.17 (m, 2H, NH + H_{arom}), 8.03 (dd, 1H, J = 7.6 Hz, H_{arom}), 7.92 (d, 1H, J = 7.6 Hz, H_{arom}), 7.61–7.57 (m, 2H, H_{arom}), 7.55–7.53 (m, 1H, H_{arom}), 7.49–7.45 (m, 1H, H_{arom}), 7.40 (dd, 1H, J = 5.9 Hz, H_{arom}), 6.87–6.85 (td, 1H, J = 8.5 Hz, H_{arom}), 6.77 (dd, 1H, J = 7.6 Hz, H_{arom}), 6.60 (td, 1H, J = 7.6 Hz, H_{arom}), 4.85 (s, 2H); ^{13}C NMR (213 MHz, DMSO d_6) δ (ppm): 159.99, 141.39, 135.17, 134.22, 131.70, 128.88, 126.39, 125.20, 124.90, 124.25, 122.99, 121.90, 121.90, 117.90, 117.41, 117.29, 116.34. Elem. Anal. for $C_{17}H_{15}N_3O$: calcd C, 73.63; H, 5.45; N, 15.15; O, 5.77; found C, 73.65; H, 5.43; N, 15.17; O, 5.75.

2.2.2. (2-(((3-hydroxynaphthalen-2-yl)methylene)amino)phenyl)-3-(naphthalen-1-yl)urea (HL)

1.77 g (10 mmol) of aminodiarylurea in 20 mL of ethanol added to a solution of 2-hydroxynaphthaldehyde (2.58 g, 15 mmol) in 20 mL of ethanol. The mixture was stirred 30 min at room temperature and then heated 18 h under reflux. The reaction progress was monitored by TLC using diethyl ether/petroleum ether (70/30) as eluent. The reaction mixture was filtered and the crude solid was purified by recrystallization from ethanol.

Light yellow, yield: 82%; M.p.243–245 °C; IR (cm^{-1}) *v*: 3286(NH), 1643(C = O), 1572(C = N); 1547(C = C); ^{1}H NMR (850 MHz, DMSO d_6) δ(ppm): 15.12 (s, 1H, OH), 9.69 (s, 1H, NH), 9.22(s, 1H, NH), 8.73 (s, 1H, CH = N), 8.57 (d, 1H, J = 8.5 Hz, H_{arom}), 8.17 (dd, 1H, J = 8.5 Hz, H_{arom}), 8.00 (d, 1H, J = 8.5 Hz, H_{arom}), 7.97 (d, 1H, J = 6.8 Hz, H_{arom}), 7.93 (t, 2H, J = 6.8 Hz, H_{arom}), 7.86 (d, 1H, J = 7.6 Hz, H_{arom}), 7.65 (t, 2H, J = 7.6 Hz, H_{arom}), 7.59–7.53 (m, 3H, H_{arom}), 7.48 (t, 1H, J = 7.6 Hz, H_{arom}), 7.40 (t, 1H, J = 7.6 Hz, H_{arom}), 7.31 (t, 1H, J = 7.6 Hz, H_{arom}), 7.23 (t, 1H, J = 7.6 Hz, H_{arom}), 7.15 (d, 1H, J = 8.5 Hz, H_{arom}); ^{13}C NMR (213 MHz, DMSO d_6) δ (ppm): 167.10, 158.92, 153.74, 138.77, 136.75, 134.74, 134.20, 133.39, 132.60, 131.72, 129.48, 128.84, 128.64, 127.52, 127.23, 126.78, 126.39, 126.13, 124.62, 124.11, 121.67, 123.33, 122.21, 121.31, 121.20, 120.20, 118.77, 110.11; Elem. Anal. for $C_{28}H_{21}N_3O_2$: calcd C, 77.94; H, 4.91; N, 9.74; O, 7.42; found C, 77.91; H, 4.93; N, 9.72; O, 7.44.

2.2.3. Preparation of complexes

To a solution of urea Schiff base **HL1 (1)** (1.5 mmol) in 20 mL of ethanol was added an ethanolic solution of 1.5 mmol metal chloride ($NiCl_2{\cdot}6H_2O$, $CoCl_2{\cdot}6H_2O$, $FeCl_3{\cdot}6H_2O$, $CuCl_2{\cdot}2H_2O$, $ZnCl_2$, $CrCl_3{\cdot}6H_2O$, $MnCl_2{\cdot}3H_2O$) in L:M molar ratios of 1:1. The reaction mixture was stirred at room temperature for 30 mn and the reaction mixture was refluxed for 3 h. The progress of reaction was monitored with TLC (DMF/ethanol: 20/80). At the end of the reaction, the mixture was cooled, filtered, washed many times with hot ethanol to remove the non-reacting organic materials and dried under vacuum.

Ni(II) complex: Yellow, yield: 80%, Mp: 320 °C, IR: ν (cm^{-1}): 3650 (br), 3272 (m), 3263 (m), 1647 (s), 1580 (s), 1596 (m), 631 (s), 551 (s), 451 (s). UV–Vis (ethanol), λ_{max} (nm): 490, 380, 330, 320, 290. Elemental Analysis: calcd C, 58.12; H, 4.53; N, 7.26. Found: C, 58.11; H, 4.50; Cl, N, 7.23. Molar conductivity Λ_m (DMF): 12.8 Ω^{-1} cm^2 mol^{-1}.

Fe (III) complex: Brown, yield: 77%, Mp > 350 °C, IR: ν (cm^{-1}): 3270 (m), 3260 (m), 1650 (s), 1619 (s), 1595 (s), 691 (s), 527 (s), 410 (s). UV–Vis (ethanol), λ_{max} (nm): 460, 440, 380, 310, 260. Elemental analysis (%): calcd C: 56.69, H: 4.08, N: 7.08, Found C: 56.67, H: 4.06, N: 7.05. Molar conductivity Λ_m (DMF): 14.2 Ω^{-1} cm^2 mol^{-1}.

Cu (II) complex: Red, yield: 85%, Mp: 305 °C, IR: ν (cm^{-1}): 3660 (br), 3272 (m). 3270 (m), 3262 (m), 1650 (s), 1575 (s), 1597 (m), 645 (s), 630 (s), 408 (s). UV–Vis (ethanol), λ_{max} (nm): 500, 380, 330, 310, 260. Elemental analysis (%): calcd C: 55.87, H: 4.19, N: 6.98, Found C: 55.86, H: 4.16, N: 6.95. Molar conductivity Λ_m (DMF): 20.3 Ω^{-1} cm^2 mol^{-1}.

Co (II) complex: Red, yield: 78%, Mp > 350 °C, IR: ν (cm^{-1}): 3650 (br), 3268 (s), 3265 (m), 3263 (s), 3260 (m). 1647 (s), 1620 (s), 1575 (s), 1593 (m), 694 (s), 520 (s), 400 (s). UV–Vis (ethanol), λ_{max} (nm): 470, 320, 310, 255. Elemental analysis (%): calcd C: 56.30, H: 4.22, N: 7.03, Found C: 56.29, H: 4.21, N: 7.01. Molar conductivity Λ_m (DMF): 14.7 Ω^{-1} cm^2 mol^{-1}.

Mn (II) complex: Light Red, yield: 75%, Mp: 298 °C, IR: ν (cm^{-1}): 3400 (br), 3280 (s), 3275 (m), 3265 (s), 3250 (m). 1649 (s), 1636 (s), 1590 (s), 687 (s), 549 (s), 398 (s). UV–Vis (ethanol), λ_{max} (nm): 550, 470, 350, 260. Elemental analysis (%): calcd C: 58.50, H: 4.56, N: 7.31, Found C: 58.48, H: 4.54, N: 7.28. Molar conductivity Λ_m (DMF): 24.7 Ω^{-1} cm^2 mol^{-1}.

Zn (II) complex: Light yellow, yield: 85%, Mp: 285 °C, IR: ν (cm^{-1}): 3600 (br), 3270 (s), 3275 (m), 3259 (s), 1650 (s), 1617 (s), 1594 (s), 692 (s), 519 (s), 405 (s). UV–Vis (ethanol), λ_{max} (nm): 580, 450, 380, 270. Elemental analysis (%): calcd C: 59.28, H: 4.26, N: 7.41, Found C: 59.25, H: 4.24, N: 7.39. Molar conductivity Λ_m (DMF): 13.6 Ω^{-1} cm^2 mol^{-1}.

Cr (III) complex: Red, yield: 70%, Mp: 270 °C, IR: ν (cm^{-1}): 3270 (s), 3262 (m), 1650 (s), 1616 (s), 1592 (s), 695 (s), 656 (s), 617 (s), 409 (s). UV–Vis (ethanol), λ_{max} (nm): 450, 370, 255. Elemental analysis (%): calcd C: 57.06, H: 4.10, N: 7.13, Found C: 57.03, H: 4.08, N: 7.11. Molar conductivity Λ_m (DMF): 28.2 Ω^{-1} cm^2 mol^{-1}.

2.3. In vitro anticancer activities

2.3.1. Cell culture

The American type culture collection provided human cell lines, prostate adenocarcinoma (PC-3), ovarian adenocarcinoma (SKOV3), and cervical cancer cell line (HeLa) (ATCC). In a humidified, 5% (v/v) CO_2 condition, cells were incubated in RPMI-1640 enriched with (100 g/mL); penicillin (100 units/

L); and heat-inactivated foetal bovine serum (10 percent v/v) at 37 °C (OECD, 2001).

2.3.2. Cytotoxicity assay (assay for cellular toxicity)

Using the Sulphorhodamine B assay, the cytotoxicity of chemical compounds was assessed against human tumor cells (PC-3, SKOV3, and HeLa) (SRB). Before being treated with the chemical compounds, 80 percent confluent proliferating cells trypsinized and cultivated in a 96 well tissue culture plate for 24 h. Untreated cells (control) added to cells that exposed to the six various concentrations of each drug (0.01, 0.1, 1, 10, 100, and 1000 g/ml). The cells were also given doxorubicin, and they were exposed to the doses for 72 h before being fixed with TCA (10% w/v) for 1 h at 4 °C. After repeated washes, cells were stained for ten min in the dark with a 0.4% (w/v) SRB solution. Glacial acetic acid, 1 percent (v/v), is used to remove any remaining discoloration. The SRB-stained cells dissolved in Tris-HCl after drying overnight, and the color intensity was quantified in a microplate reader at 540 nm. Using SigmaPlot 12.0 software, the correlation between viability percentage of each tumor cell line and chemical concentrations was analyzed to determine the IC_{50} (drug dose that reduces survival to 50%). (Ghfar et al., 2021, Alam et al., 2021).

2.4. In vivo acute oral toxicity assessment

In the current study, seven urea Schiff base complexes and parent urea schiff base were evaluated their median lethal dose (LD_{50}) and five female rats were used for each compound. The average of an animal's body weight was 135.9 ± 9.4. The animals were purchased from the Laboratory Animal Centre of the Qassim University (QU), Saudi Arabia. The rats were randomly selected and housed in polypropylene cages (5 rats/cage) for a week before dosing to adapt to laboratory conditions. The animals were kept under a standard condition in a ventilated room with a steady light (12 hr): dark (12 hr) cycle and temperature (24 ± 2 °C). The standard food pellets (1st Milling Company, Qassim) and water were provided *ad libitum*. All experimental procedures on animals were conducted according to the regulations of the Research Unit, College of Pharmacy Unaizah, and Qassim university's roles and regulations. The Committee of Research Ethics, Deanship of Scientific Research, QU (Ethics number 20-02-02), approved all the experimental procedures.

Acute oral toxicity (LD_{50} evaluation):

To evaluate the safety use, an acute oral toxicity test was used to determine the median lethal dose (LD_{50}) for each synthesized Schiff-based urea hybrid compound-complex. According to the Organization for Economic Co-operation and Development (ORCD) guideline for testing chemicals (OECD, 2001). After overnight fasting with access to water, the animals were fed orally with a single dosage of 175, 550, 1000, and 2000 mg/kg for each synthesized Schiff-based urea hybrid complex by oral gavage. Before dose administration, the bodyweight of each animal was determined, and the dose was calculated according to body weight. For the vehicle control group, 0.5 DMSO was administered. Feeding was started 3–4 hrs after dosing, and animals were observed at 30 min, 2, 4, 8, 24, and 48 hrs up to 14 days to monitor any toxicological signs or mortality after 14 days.

2.5. Statistics

Data were analyzed using SPSS software version 23 (SPSS, Inc, Chicago, USA). Numeric parametric data were presented in the mean and standard error of mean. One-way ANOVA followed by post-hoc Dunant test (less than ligand) was used for comparing IC_{50} and bodyweight of the animal for Urea Schiff-based complex compounds with urea Schiff base. The P-value < 0.05 was considered statistically significant.

3. Results and discussion

3.1. Chemistry

Our strategy started with the synthesis of ligand **HL** via the condensation in equimolar amounts of *o*-phenylenediamine and naphthyl isocyanate in anhydrous dichloromethane under catalyst-free conditions. The reaction afforded the aminodiarylurea in good yield (90%) after purification following Scheme 1. Aminodiarylurea was converted into the corresponding urea Schiff base **HL 1** in the presence of 2-hydroxynaphthaldehyde under reflux (Scheme 1).

The metal complexes were synthesized in L:M ratios 1:1 (Scheme 2) via the reaction of ethanolic solution of ligand **HL (1)** and metal chloride salts ($NiCl_2{\cdot}6H_2O$, $FeCl_3{\cdot}6H_2O$, $CuCl_2{\cdot}2H_2O$, $CoCl_3{\cdot}6H_2O$, $MnCl_2{\cdot}3H_2O$, $ZnCl_2$, $CrCl_3{\cdot}6H_2O$). The target metal complexes were characterized by FT-IR spectroscopy, UV–Vis electronic absorption, elemental analysis, Thermal analysis, X-ray powder diffraction, and SEM, as well as molar conductivity and magnetic susceptibility study.

3.1.1. ^1H and ^{13}C NMR spectra

^{1}H NMR spectrum of ligand **HL** exhibited downfield singlet at 15.12 ppm attributed to hydroxyl phenolic proton. The spectrum also manifest two singlets at 9.52 and 8.92 ppm, respectively corresponding to NH of urea moiety. At 8.54 ppm, the azometine proton appeared as a doublet. The other aromatic protons were detected in the common region of aromatic protons at δ_H 8.28–7.01 ppm. The ^{13}C NMR of compound **5f** indicated a singlet for hydroxyl carbon at 167.1 ppm and a singlet for the urea moiety carbonyl group at 161.59 ppm. The additional aromatic carbons appeared in the usual aromatic region at δ_C 153.7–110.1 ppm.

3.1.2. Molar conductivity measurements

The molar conductance values of the complexes in DMF (10^{-3}M) are in the range of 12.8–28.2 Ω^{-1} cm^2 mol^{-1} (Table 1), the low values indicate the non-electrolytic nature of the complexes (Al-Hakimi et al., 2011; El-saied et al., 2020; El-Tabl et al., 2012). This confirms that the anion is coordinated to the metal ion.

3.1.3. Magnetic moments susceptibility

Room temperature magnetic moments of the complexes **(2–8)** was summarized in Table 1. Ni(II) complexes **(2)** show paramagnetic values (2.75 BM) confirming octahedral geometry around the Ni(II) ion. Fe (III) complex (3) shows a value 5.66B.M, indicating high spin iron(III) octahedral geometry. Complex **(4)** shown value (1.73B.M.) indicating octahedral

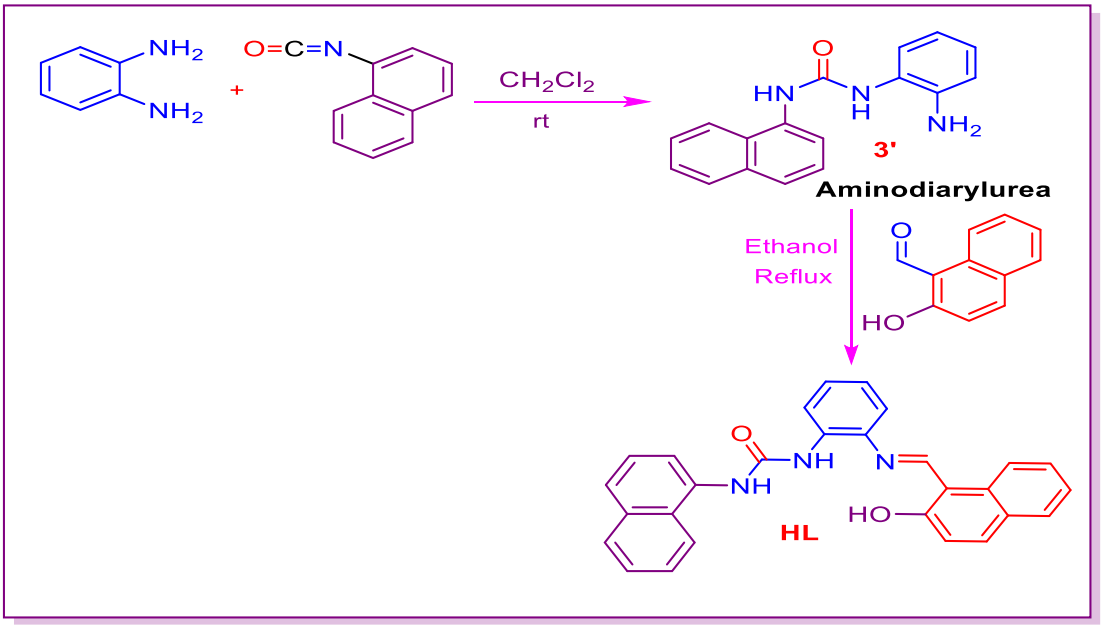

Scheme 1 Synthesis of urea Schiff base **HL.**

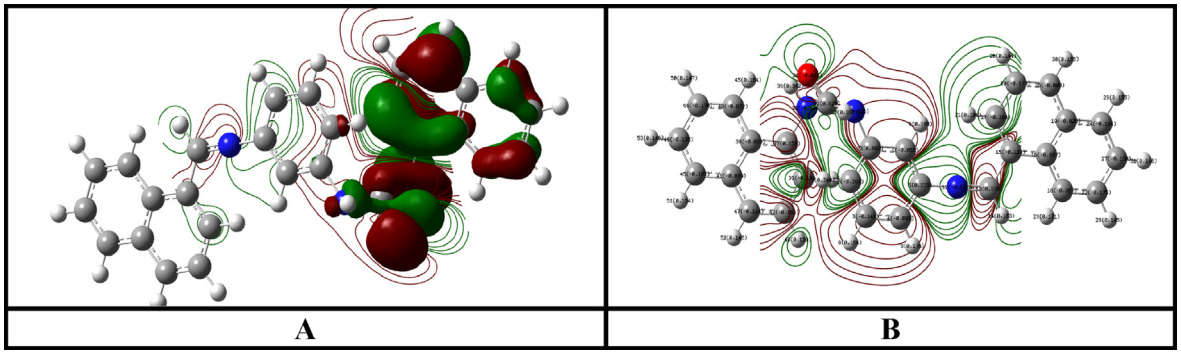

Fig. 2 **(A)** HOMO and **(B)** LUMO of Ligand HL.

geometry around Cu(II) ion. Cobalt(III) complex **(5)** shown value 4.2B.M. (Table 1), indicating high spin octahedral cobalt(II) complex. The magnetic moment value for manganese(II) complex **(6)** is 4.92B.M. suggest high spin octahedral geometry around the manganese(II) ion. Small value of the magnetic susceptibility here is due to electron – electron interaction (Al-Hakimi et al., 2011, Al-Hakimi et al 2020, Buldurun et al., 2021). zinc(II) complexes **(7),** and cadmium (II) complex **(9)** show diamagnetic values. Chrome complex **(8)** shown value 1.82B.M indicating low spin octahedral geometry around Cr(III) ion.

3.1.4. Infrared spectra

Infrared Spectra is one of the important techniques through which we identify the functional groups of chemical compounds. In addition, this technique makes it possible to identify the bonding points between the studied ligands and metal ions in the complexes. In this study, the ligand **HL** showed various vibrations at different values indicating the existing functional groups on the ligand. The ligand showed a sharp vibration band in the value 3500 cm^{-1} indicating the vibrations of the phenolic hydroxyl group (Table 2). In addition, two vibration bands appeared at the values 3272 cm^{-1} and 3260 cm^{-1}, indicating the vibrations of (NH) group, while the vibrations of the carbonyl group (C = O) appeared at the value 1647 cm^{-1}. As for the (N = CH) azomethine group, it appeared at a value of 1616 cm^{-1}, while the infrared spectrum showed vibration bands at 1576 cm^{-1} indicating the vibrations of the bonds (C = C).

As in complexes (2), (3), (6) and (8), the ligand behavior in metal complexes is monobasic bidentate in which the ligand bonded to the metals ions through the enolic hydroxyl group, and azomethine (C = N) group through nitrogen atoms (Table 2). This bonding behavior was confirmed by disappearance the bands characteristic of hydroxyl group ν(OH) in all complexes. On the other hand, the ligand behavior neutral bidentate as in complexes **(4)** and **(5)** in which the ligand coordinated to the metals ions through the oxygen of hydroxyl group, and azomethine (C = N) group through nitrogen atoms.

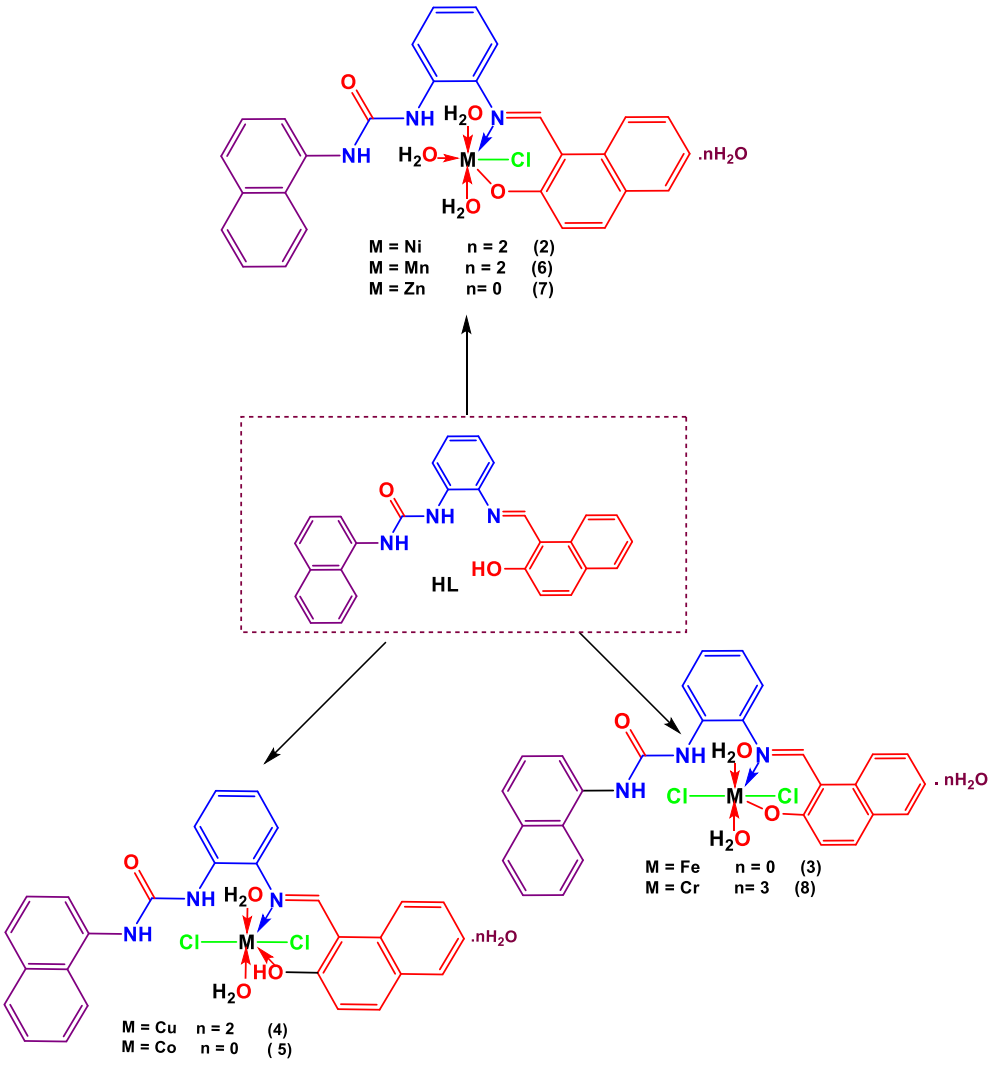

Scheme 2 Synthesis of urea Schiff base complexes.

The metal complexes also present vibration bands ranging 3265–3600 cm^{-1} indicating the vibrations of water molecules. The vibrations of the hydroxyl group associated with the metal ion appeared at the values of 3480 and 3450 cm^{-1}, respectively, as a sharp and a medium band. It also mentioned a shift in the vibrational bands of the azomethine group between (1595–1611) cm^{-1} indicating the bonding of metal ions through the nitrogen atom in the group. The metal complexes also showed vibration bands between (631–695) cm^{-1}, (520–567) cm^{-1} and (401–410) cm^{-1} indicating the vibrations of ν(M−O), ν(M−N) and ν(M−Cl) respectively (Al-Hakimi, 2020; Shakdofa et al., 2017; El-Saied et al., 2018).

3.1.5. UV– vis spectra

The ligand **HL1 (1)** showed absorption bands at 390, 300 and 220 nm indicating to the electronic transitions of free electrons on nitrogen and oxygen atoms, π electrons and σ electrons so that the transitions were n → π*, π → π * and σ → σ * respectively (Table 3). As for the metal complexes, there has been a shift of these absorption bands and the emergence of other absorption bands that indicate the characteristic electronic transitions of the transition metals represented by d-d transitions.

In the nickel (II) complex **(2)**, absorption bands appeared in the visible region at the values of 490 and 380 nm due to electronic transitions $^3A_{2g}(F) \rightarrow {}^3T_{1g}(P)$ (υ_1), $^3A_{2g}(F) \rightarrow {}^3T_{1g}(F)$ (υ_2) respectively indicating an octahedral nickel(II) complex. On other hand, the complex **(3)** for iron (III) showed absorption bands at the values of 510, 440 and 380 nm indicating that the two and three bands are due to charge transfer transition while the first band is considered to arise from the $^6A_1 \rightarrow {}^4T_1$ transition, these bands suggest, distorted octahedral geometry around the iron(III). The copper complex **(4)** also showed two absorption bands in the visible region at 500 and 390 nm indicating to $^2B_1 \rightarrow {}^2E$ and $^2B_1 \rightarrow {}^2B_2$ transitions. The deformed octahedral shape around the Cu(II) ion is shown by these transitions.

The cobalt complex **(5)** showed two absorption bands at 520 and 380 nm due to electronic transitions ^4T_1g (F) → ^4T_1g (P) and ^4T_1g (F) → ^4A_2g transitions respectively, corresponding to cobalt (II) octahedral complex. The metal complex **(6)** showed absorption bands at 550, 470 and 390 nm (Table 3), indicating to the electronic transitions $^6A_1g \rightarrow {}^4E_g$,

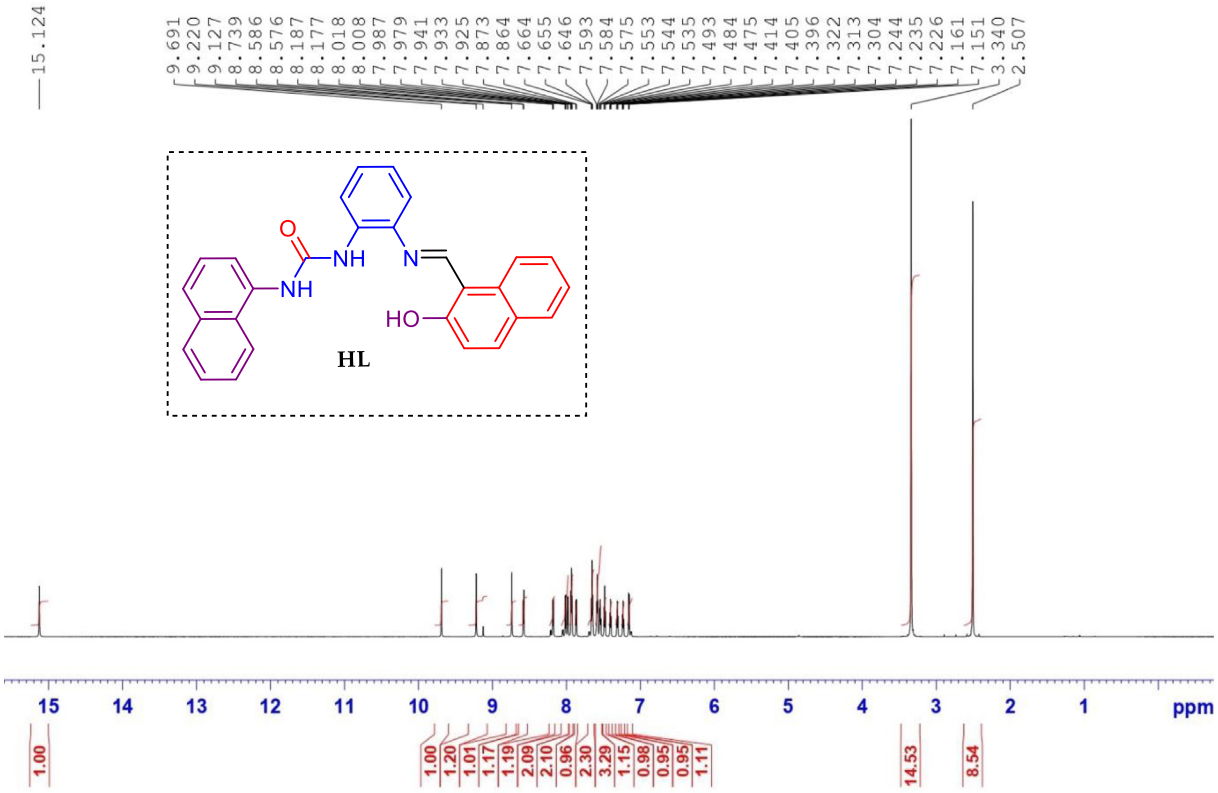

Fig. 3 ^{1}H NMR spectrum of compound ligand **HL.**

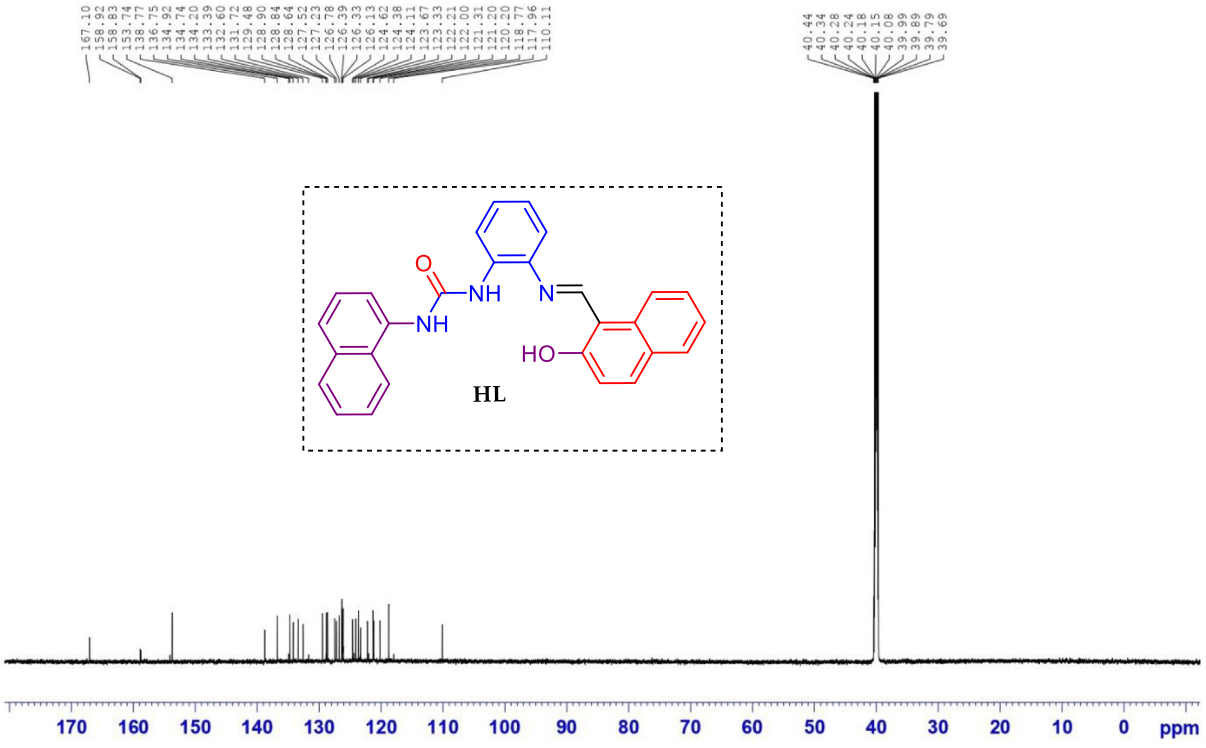

Fig. 4 ^{13}C NMR spectrum of compound ligand **HL.**

Table 1 Analytical and some physical characteristics for the ligand and its metal complexes.

N.	Comp.	Color	M.Wt.	Calc. (Found)%				Λ_M^a	Yield
				C	H	N	M		(%)
1	HL ($C_{28}H_{21}N_3O_2$)	Light Yellow	431.50	77.94(77.92)	4.91(4.89)	9.74(9.72)	—	———	80
2	$C_{28}H_{26}ClN_3NiO_5$	Yellow	578.68	58.12(58.11)	4.53(4.50)	7.26(7.23)	10.14	12.8	80
3	$C_{28}H_{24}Cl_2FeN_3O_4$	Brown	593.26	56.69 (56.67)	4.08(4.06)	7.08 (7.05)	9.41	14.2	77
4	$C_{28}H_{25}Cl_2CuN_3O_4$	Red	601.97	55.87 (55.86)	4.19(4.16)	6.98(6.95)	10.56	20.3	85
5	$C_{28}H_{25}Cl_2CoN_3O_4$	Red	597.36	56.30 (56.29)	4.22(4.21)	7.03(7.01)	9.87	14.7	78
6	$C_{28}H_{26}ClMnN_3O_5$	Light Red	574.92	58.50 (58.48)	4.56(4.54)	7.31 (7.28)	9.56	24.7	75
7	$C_{28}H_{24}ClN_3O_4Zn$	Light yellow	567.35	59.28 (59.25)	4.26(4.24)	7.41 (7.39)	11.17	13.6	85
8	$C_{28}H_{24}Cl_2CrN_3O_4$	Red	589.41	57.06 (57.03)	4.10(4.08)	7.13(7.11)	8.82	28.2	70

Table 2 IR spectra (assignments) of the Ligand (1) and its metal complexes.

No.	ν (OH)	ν(lattice H_2O) and Coord).	ν (NH)	ν (C = O)	ν(C = N)	ν(C = C)$_{Ar}$	ν(M−O)	ν(M−N)	ν(M−Cl)
(1)	3321	———	3272, 3260	1646	1616	1576	———	———	———
(2)	———	3650–3000	3272,3263	1647	1580	1596	631	551	415
(3)	———	———	3270,3262	1650	1575	1597	645	630	408
(4)	———	3660–3270	3272,3260	1650	1619	1597	691	527	410
(5)	3260–2980	3650–3265	3268,3263	1647	1620	1593	694	520	400
(6)	3400–3250	3670–3280	3275,3259	1649	1636	1590	687	549	398
(7)	———	3600–3270	3270,3265	1650	1617	1594	692	519	405
(8)	———	———	3270,3262	1650	1616	1592	695, 656	617	409

Table 3 Electronic transition of the ligands and their metal complexes in ethanol.

No.	Ligand / Complexes	λ_{max} (ethanol)	ε (mol^{-1} cm^{-1})
1	HL ($C_{28}H_{21}N_3O_2$)	390, 300, 220	7.7 $X10^{-3}$, 5.2 $X10^{-3}$
2	$C_{28}H_{26}ClN_3NiO_5$	490, 380, 330, 320, 290	2.5 $X10^{-4}$, 3.1 $X10^{-4}$, 2.0 $X10^{-3}$
3	$C_{28}H_{24}Cl_2FeN_3O_4$	460, 440, 380, 310, 260	4.1 $X10^{-4}$, 1.2 $X10^{-4}$, 1.2 $X10^{-3}$
4	$C_{28}H_{25}Cl_2CuN_3O_4$	500, 380, 330, 310, 260	1.5 $X10^{-4}$, 3.2 $X10^{-4}$, 1.2 $X10^{-3}$
5	$C_{28}H_{25}Cl_2CoN_3O_4$	470, 320, 310, 255	3.2 $X10^{-4}$, 3.0 $X10^{-4}$, 1.4 $X10^{-3}$
6	$C_{28}H_{26}ClMnN_3O_5$	550, 470, 350, 260	1.8 $X10^{-4}$, 2.2 $X10^{-4}$, 2.3 $X10^{-3}$
7	$C_{28}H_{24}ClN_3O_4Zn$	580, 450, 380, 270	3.1 $X10^{-4}$, 3.1 $X10^{-4}$, 4.2 $X10^{-3}$
8	$C_{28}H_{24}Cl_2CrN_3O_4$	450, 370, 255	5.3 $X10^{-3}$, 4.1 $X10^{-4}$, 4.1 $X10^{-3}$

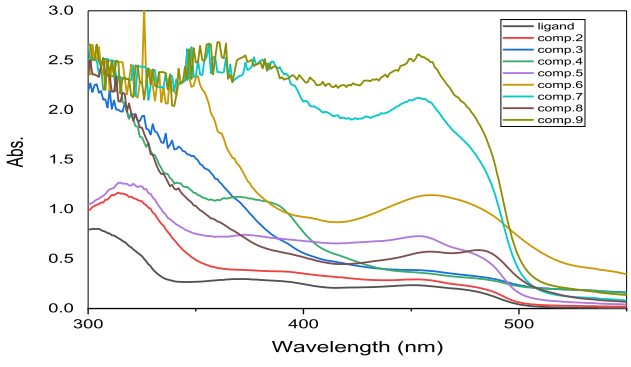

Fig. 5 UV–vis spectra of ligand and their complexes.

$^6A_{1g} \rightarrow {}^4T_{2g}$ and $^6A_{1g} \rightarrow {}^4T_{1g}$ transitions which are compatible to an octahedral geometry around the manganese(II) ion metal complexes **(7)**, and **(8)** showed various absorption bands due to LMCT transition or indicating intra ligand transitions (Al-Hakimi et al.,2011, El-Tabl et al., 2012, Shakdofa et al., 2021).

3.1.6. Thermal analysis

Thermal study of the Schiff base ligand HL and its metal complexes was carried out to determine its thermal stability. Also, to confirm whether the status of the water inside or outside the central metal ion coordination spheres. The thermo gravimetric analysis (TGA) curves in the range of 27–800 °C indicate the stability of the complexes. The TGA results of some complexes matched the elemental analysis formula. The TGA data clearly showed that the complexes were decomposed in sequential processes (El-Tabl et al., 2012, Shakdofa et al., 2021, Al-Hakimi et al., 2021, Turan et al., 2021).

Complexes **2**, **4**,6 and **8** decayed in four steps. The 1st step occurred at 60–90 °C with losses of 6.25, 5.96, 6.24 and 9.20% (calcd. 6.22, 5.98, 6.26 and 9.16%, respectively) because of the sequential removal of hydrated water molecules (Table 4). The 2nd step happened in the 130–150 °C range with weight losses of 9.30, 5.95, 9.39 and 6.10% (calcd. 9.33, 5.98, 9.39 and 6.11%, respectively) as due to the elimination of coordinated water molecules. The 3rd stage happened in range of 230–250 °C with losses of 6.30, 6.10, 6.34 and 12.23 wt% (calcd 6.31, 6.06, 6.34 and 12.20%, respectively) corresponding to hydrochloride molecules were removed. The final stage occurred at (560, 550, 5650 and 590) to (620, 650, 650 and 650) °C range with weight losses of 65.20, 68.60, 63.01 and 46.54% (calcd. 65.23, 68.78, 62.89 and 64.89% respectively) for each of the three complexes respectively, corresponding to the complexes' full degeneration and transformation to metal oxides 12.91, 13.21, 15.12 and 25.79% (NiO, CuO, MnO_2 and Cr_2O_3) respectively.

Table 4 Thermal analysis of metal complexes.

Comp. No.	Loss hydrated water % at (60-90) ^{0}C Calc. (found)	Loss coordinated Water % at (130-150) ^{0}C Calc. (found)	Loss chloride % at (230-250) ^{0}C Calc. (found)	% of the remaining portionat (550- 650) ^{0}C Calc. (found)
2	6.22 (6.25) ($2H_2O$)	9.33 (9.30) ($3H_2O$)	6.31 (6.30) (HCl)	12.91 (13.01) (NiO)
3	———————	6.10(6.31) ($2H_2O$)	12.30 (12.22) (2HCl)	26.92 (26.90) (Fe_2O_3)
4	5.98(5.96) ($2H_2O$)	5.98 (5.96) ($2H_2O$)	6.06 (6.10) (2HCl)	13.21 (13.11) (CuO)
5	———————	6.02 (6.09) ($2H_2O$)	11.88 (11.84) (2HCl)	27.80 (27.76) (Co_2O_3)
6	6.26(6.24) ($2H_2O$)	9.39 (9.39) ($3H_2O$)	6.34 (6.34) (HCl)	15.13 (15.20) (MnO_2)
7	———————	9.51 (9.45) ($3H_2O$)	6.43 (6.41) (HCl)	14.33 (14.35) (ZnO)
8	9.16(9.20) ($3H_2O$)	6.11 (6.10) ($2H_2O$)	12.20 (12.23 (2HCl)	25.77 (25.77) (Cr_2O_3)

Complexes **3**, **5**, and **7** decomposed in three steps. At a temperature range 130–150 °C, the first step occurred with weight loss of 6.31, 6.09 and 9.45% (calcd. 6.10, 6.02 and 9.52%, respectively) due to the removal of coordinated water molecules (Table 4). The 2nd stage happened at a temperature range 230–250 °C with weight losses of 12.22, 11.84 and 6.41% (calcd. 12.30, 11.88, and 6.43% respectively), indicating the removal of hydrochloride molecule. The 3rd step happened between 550 and 650 °C range with weight losses of 54.65, 60.13 and 69.66% (calcd. 54.68, 60.11 and 69.70% respectively) relating to the complexes' degeneration and transformation to metal oxides 26.90, 27.80 and 14.33% respectively (calcd. 26.92, 27.76 and 14.35% respectively) (Fe_2O_3, Co_2O_3, and ZnO) respectively (Al-Hakimi et al., 2021, Alorini et al., 2022).

3.1.7. XRD analysis

The XRD measurement output data was processed and enhanced utilizing software. The crystal structure data of the complexes matched with the crystal systems.. Table 5 lists the complexes parameters of the unit cell. The differences in computed unit cell volumes were caused by the sizes of the impurities present in the base material. Notably, the ligand **(1)**, and complex **7** exhibit monoclinic crystal systems. Complex **2**, whose XRD spectrum is shown a tetragonal crystal system. Complexes 5 have orthorhombic crystal systems. On the other hand, the other complexes showed a random shape during the analysis using XRD, this may be because the powder of these samples was not in good shape (Alorini et al., 2022) (see Fig. 6).

Table 5 XRD data of ligand and their complexes.

Parameters		HL (1)	Complex 2	Complex 5	Complex 7
a (Å)	**Lattice constant**	12.320(19)	8.318(13)	11.6(2)	31.58(11)
b (Å)		23.41(3)	31.24(4)	11.5(3)	3.950(11)
c (Å)		11.01(2)	14.31(3)	10.0(4)	19.86(3)
α (°)	**Inter axial angle**	90	90	115.6(13)	90
β (°)		90.1(3)	93.69(12)	104.0(19)	90
γ (°)		90	90	73.4(16)	90
Crystal system		Monoclinic	Tetragonal	Orthorhombic	Monoclinic
Space group		*P2*	*P4*	*P2*	*P2*
Unit cell Volume (Å^3)		3177(9)	3710(11)	1145(55)	2478(12)
Crystallite Size		80(9)	177(28)	21(2)	86

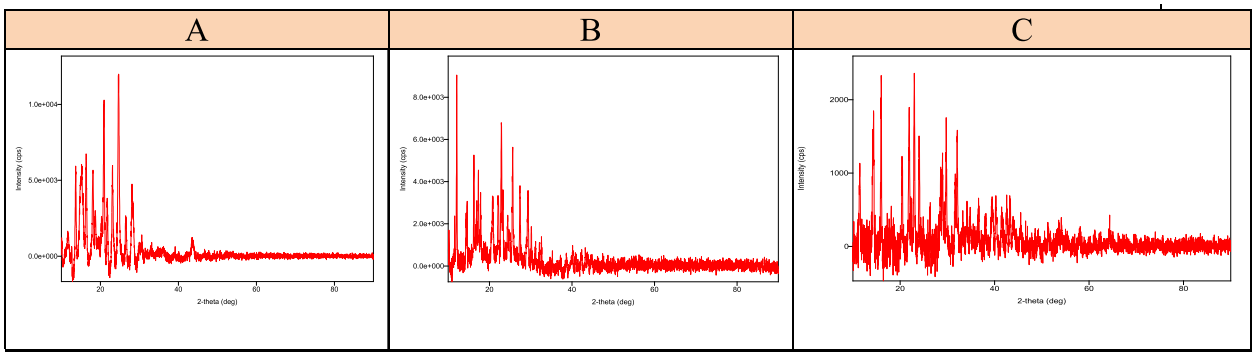

Fig. 6 A: XRD of ligand (**1**), B: XRD of nickel complex (**2**) and (C) XRD of cobalt complex (**5**).

3.1.8. SEM analysis

The studied compounds showed various shapes when analyzed using the SEM (Fig. 7). The ligand **HL 1** appeared in a sticky shape, while the complexes **2** and **7** appeared in a spherical shape, and the complex **5** appeared randomly (Alorini et al., 2022) (see Figs. 7-11).

3.2. Anticancer study

The in *vitro* anticancer studies of ligand **HL 1** and metal complexes **2**–**8** were screened against three cancer cell lines **PC3** (prostate), **SK-OV-3** (ovarian), and **HeLa** (cervical), SBR tests with six different concentrations of each chemical (0.01, 0.1, 1, 10, 100, and 1000 mg/mL) were used to calculate IC50. The results in Table 6 indicate that tested compounds in the actual study manifested higher cytotoxic activity against selected human cancer cells than those described in previous studies (Matela et al., 2020, Poyraz et al., 2017).

Mentioned in the Table 6, both Nickel complex **2** and Iron complex **3** were more active than ligand **HL 1** toward three cancer cells. Nickel complex displayed a moderate activity against PC3, SK-OV-3 and HeLa cancer cells with IC_{50} value of 6.56 ± 0.56, 7.17 ± 1.89 and 5.83 ± 2.00 μg/mL respectively. Also, iron complex increase the activity and present a strong efficiency than ligand HL 1 with IC_{50} value of 5.05 ± 0.66, 9.32 ± 0.81 and 5.44 ± 0.60 μg/mL toward PC3, SK-OV-3 and HeLa respectively.

Cobalt complex **5,** display weak activity against cancer cells PC3 with IC_{50} value of 18.89 ± 1.70 and μg/mL in comparison with the free ligand **1** with IC_{50} value of 8.71 ± 0.50 μg/mL, exhibited a moderate activity toward HeLa with IC_{50} of 6.67 ± 0.80 and manifested a strong inhibition growth against **ovarian cancer cell** SKOV3 with IC50 value of **0.73 ± 0.06** μg/mL. Chromium complex **8** presented a moderate activity against human prostate cancer cell line PC3 and increase considerably the activity toward **ovarian cancer cell SKOV-3** and **cervical cancer cell HeLa** with

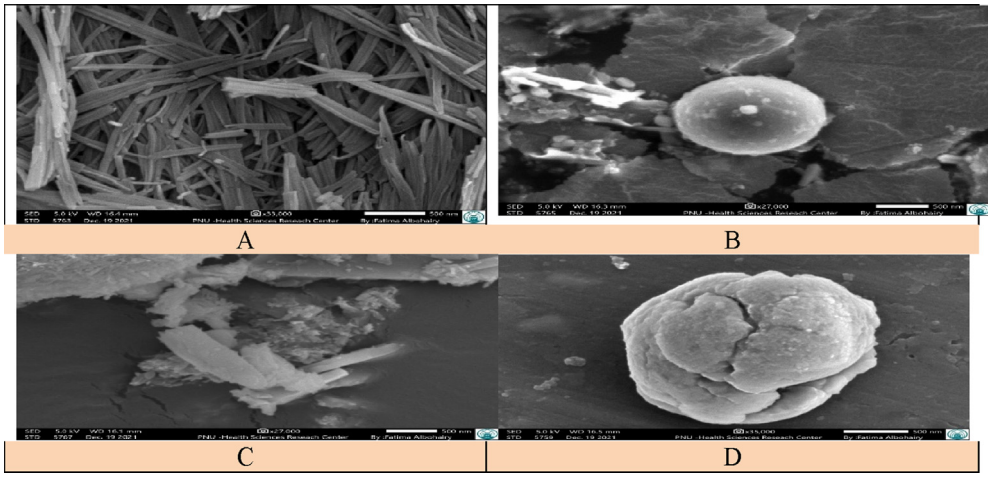

Fig. 7 SEM image of compounds: A: ligand HL (**1**), B: nickel complex (**2**), C: cobalt complex (**5**) and D: zinc complex (**7**).

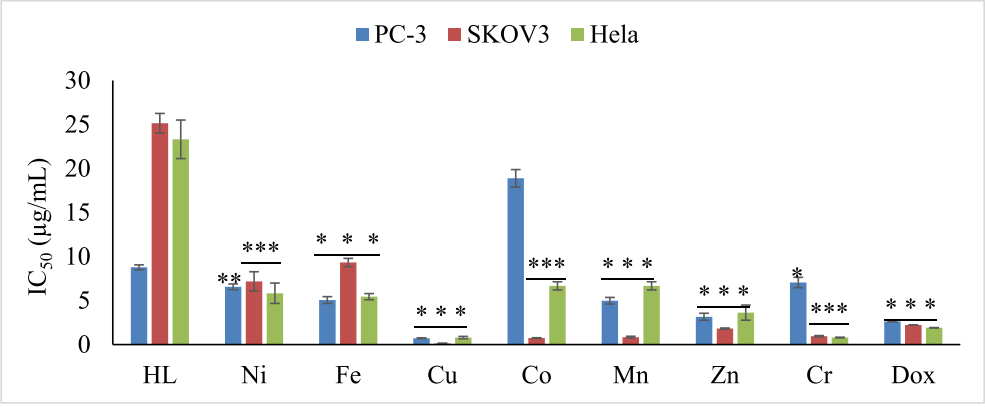

Fig. 8 in vitro antiproliferative activities of ligand and its complexes against **PC3, SKOV-3**, and **HeLa** cancer cells. Data represents as mean ± SEM for three replications. Significant between ligand and its complexes at different cancer cell was tested by adopting one way ANOVA followed by post-hoc Dunant test (less than ligand) ($P < 0.05$; * $P < 0.05$; ** $P < 0.01$; *** $P < 0.001$).

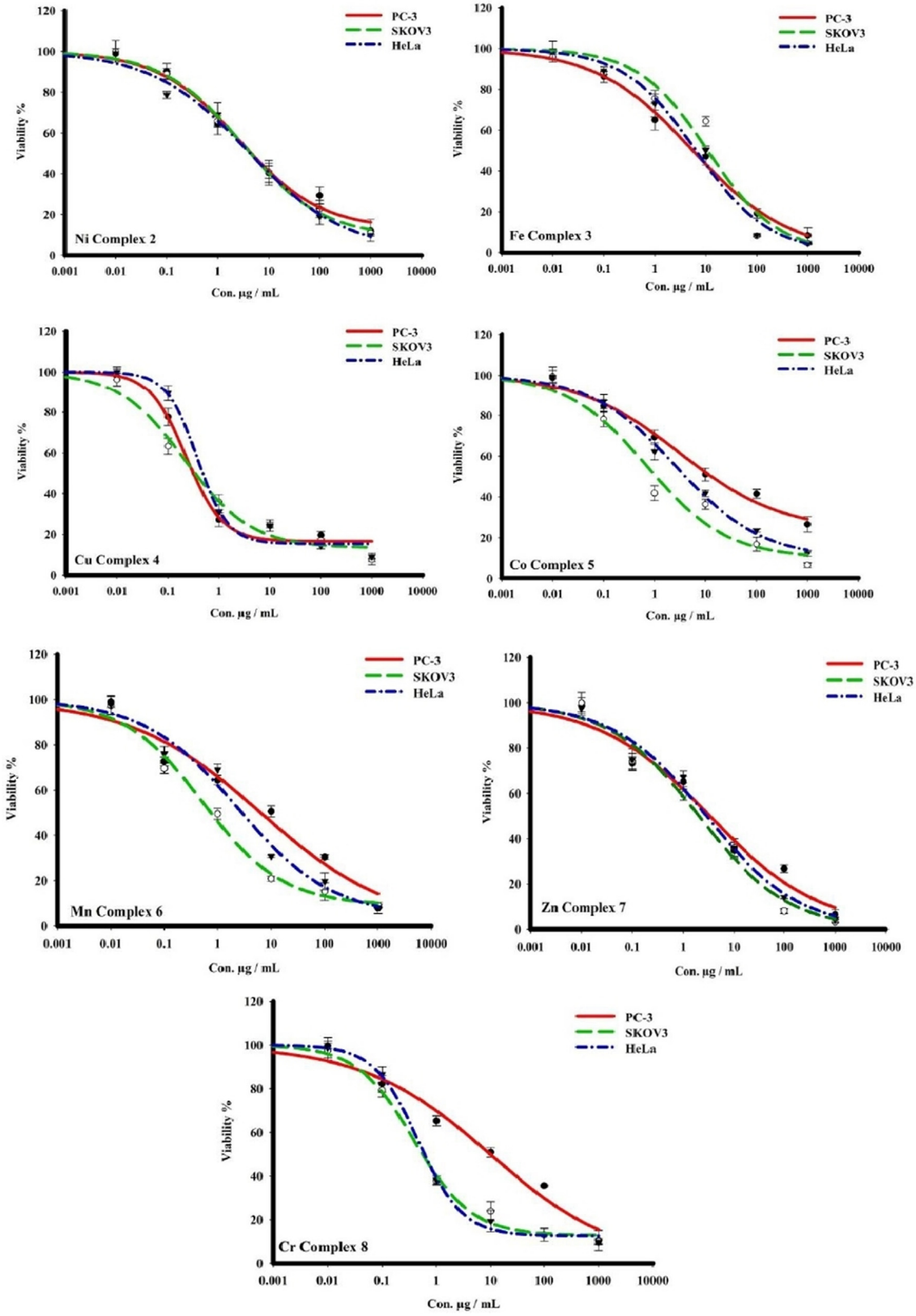

Fig. 9 The dose–response curves cytotoxicity of complexes towards PC3, SKOV-3, and HeLa human cell lines. Cells were exposed to metal complexes with different concentrations for 72 h. Cell viability was determined by SRB stain.

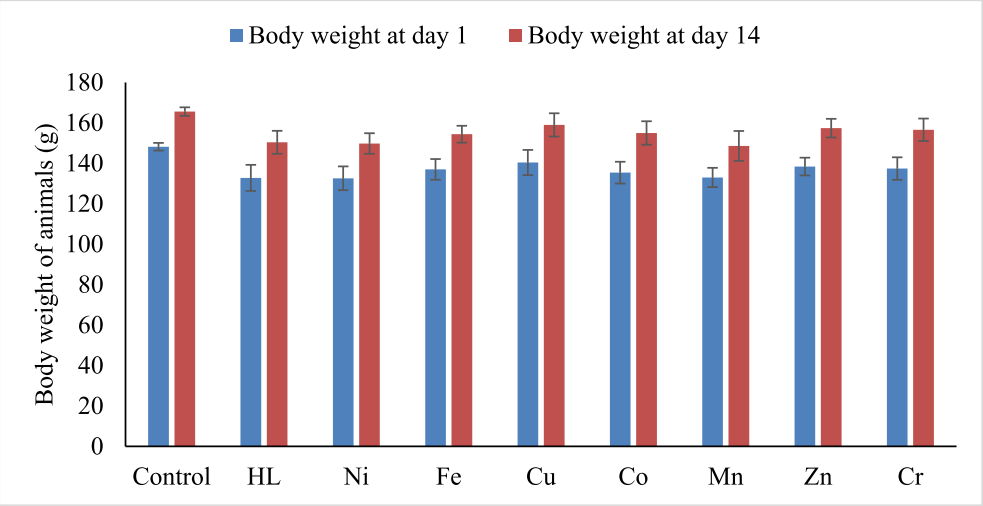

Fig. 10 The body weight of animals on day 1 of the experiment and at the end of observation day 14. The data represent mean ± SEM. No significant **occurred in body weights of animals for control, the ligand (HL) and its complexes.**

Table 6 The IC50 values (μg/mL) of the evaluated ligand **HL 1** and its metal complexes **2–9** screened for human cancer cells **PC3**, **SK-OV-3** and **HeLa.**

	Compound	IC$_{50}$ (μg/mL)*		
		PC3	SK-OV-3	HeLa
(1)	HL ($C_{28}H_{21}N_3O_2$)	8.71 ± 0.50	25.12 ± 1.91	23.32 ± 3.71
(2)	$C_{28}H_{26}ClN_3NiO_5$	6.56± 0.56	7.17±1.89	5.83± 2.00
(3)	$C_{28}H_{24}Cl_2FeN_3O_4$	5.05 ± 0.66	9.32±0.81	5.44 ± 0.60
(4)	$C_{28}H_{25}Cl_2CuN_3O_4$	0.71 ± 0.06	0.12±0.06	0.79 ± 0.23
(5)	$C_{28}H_{25}Cl_2CoN_3O_4$	18.89 ± 1.70	0.73±0.06	6.67 ± 0.80
(6)	$C_{28}H_{26}ClMnN_3O_5$	4.98± 0.65	0.84±0.17	3.62 ± 1.48
(7)	$C_{28}H_{24}ClN_3O_4Zn$	3.16± 0.68	1.82±0.10	5.02 ± 0.75
(8)	$C_{28}H_{24}Cl_2CrN_3O_4$	7.05 ± 1.01	0.95±0.11	0.79 ± 0.06
	Dox	2.6 ± 0.03	2.2 ± 0.02	1.9 ± 0.04

*Each data represents mean and standard deviation of three replicates. Cells were exposed to metal complexes with different concentrations for 72 h. Cell viability was determined by SRB stain.

IC50 value of **0.95 ± 0.11** and **0.79 ± 0.06** μg/mL respectively.

Regarding Fig. 5, both manganese complex **(6)** and zinc complex **(7)** presented a moderate activity against anticancer cells PC3 and Hela and exert an excellent anti-proliferation activity toward **ovarian cancer** cell SKOV-3 with IC$_{50}$ value of **0.84 ± 0.17, 0.12 ± 0.06** and **1.82 ± 0.10 μg/mL** respectively compared with **Dox** (2.2 ± 0.02 μg/mL).

Consulting Fig. 5, it is clear that copper complex **4** evolved the best results **against three cancer cells** PC3, SKOV3, and HeLa, and manifested an excellent activity with IC$_{50}$ values of **0.71 ± 0.06, 0.12 ± 0.06**, and **0.79 ± 0.23** μg/mL, respectively in accordance with previous reports (Hernández-Romero et al., 2021) and also manifested higher activity than standard drug reference Dox (See Table 6).

It is worth to mention, that most synthesized complexes demonstrate higher efficiency than clinically used drug such as cisplatin (IC$_{50}$ ~ 2.4 μg /mL) (Ray et al., 2007), estramustine (IC$_{50}$ ~ 0.35 μg /mL) (Nicholson et al., 2002) and etoposide (IC$_{50}$ ~ 17.4 μg /mL) (Hernández-Romero et al., 2021).

For the most active complex, copper complex exhibited cytotoxity activity against HeLa cancer cell more active than analog compounds in previous studies (Kumaravel et al., 2018). The copper complex displayed also excellent activity toward SK-OV3 cancer cell, while analogs in other studies was inactive (Sukanya et al., 2018; Yang et al., 2016).

In summary, most of synthesized complexes displayed stronger inhibition growth of cancer cell than ligand HL 1 approving that incorporation of metal considerably enhances the anti-proliferative against three cancer cells PC3, SKOV3, and HeLa. The best result was observed with copper complex which is considered the most effective of this series exhibiting an excellent activity against three cancer cells and it is considered more active than clinically used drug doxorubicin. It is explicit to remark that majority of target synthesized complexes except for nickel and iron complexes manifested an excellent activity, especially toward ovarian cancer cell line SKOV-3 with IC$_{50}$ values of **0.73 ± 0.06, 0.84 ± 0.17, 1.82 ± 0.10, 0.95 ± 0.11,** and **0.12 ± 0.06 μg/mL** for cobalt, manganese, zinc, chrome and copper complexes respectively

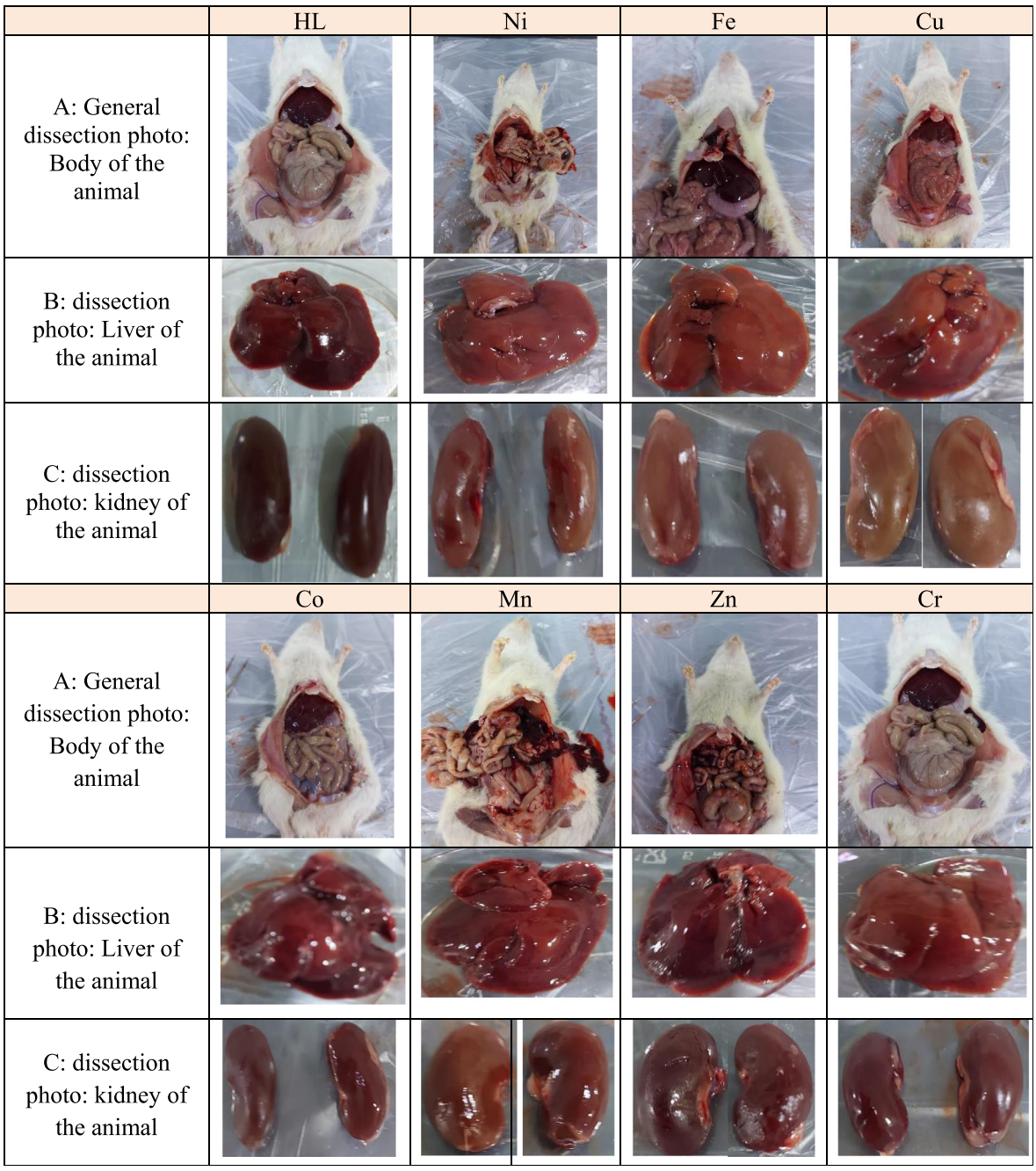

Fig. 11 Dissection Photos of animals after 14 days of the experiment, A:: General dissection photo: Body of the animal dissection photo of animal, B: B: dissection photo: Liver of the animal C: C: dissection photo: kidney of the animal.

compared with **Dox** (2.2 ± 0.02 μg/mL) which authorize promoters to use them as candidate anticancer agents.

3.3. In vivo acute oral toxicity assessing

All urea Schiff based hybrid complex and control induced no significant toxicity in *in vivo* experiment.

The rats were treated once either with urea Schiff-base hybrid complex (suspended in 0.5 DMSO) at the range of dosages of 175, 550, 1000, and 2000 mg/kg were used. After 14 days of the experiment, no mortality was observed, and all the rats were alive during the treatment period. There were no significant changes in body weight or gross appearance of liver and kidneys on the experimental animals. Neither physical abnormalities nor behavioral changes were observed during the treatment period when compared whith control group. The LD_{50} is more than 2000 mg/kg in female rats.

4. Conclusion

Physicochemical techniques were used to analyze mononuclear complexes 2–8 containing hybrid Urea Schiff base HL that were prepared using a range of metal chloride salts in L:M ratios of 1:1. The low molar conductance value implies that

the complexes are non-electrolytic and confirms the coordination of ions to metal complexes. The results further show that the ligand HL forms an octahedral geometry with metal ions as a monobasic or neutral monodentate chelator via the nitrogen of azomethine and the deprotonated/protonated phenolic oxygen atom. The XRD study of the ligand and its complexes revealed a monoclinic, tetragonal, orthorhombic, and hexagonal system, which corresponded to the urea Shiff base (1) and zinc, nickel, and cobalt complexes, respectively. Based on the findings of this study's cytotoxicity and toxicity evaluations, it can be stated that the ligand has modest activity. Nickel and iron complexes have moderate inhibition against three cancer cells: PC3, SKOV3, and HeLa. Copper complexes produced the greatest effects, with IC50 values of 0.72 0.04, 0.12 0.04, and 0.79 0.13 g/mL, respectively, against three cancer cells PC3, SKOV3, and HeLa. Furthermore, *in vivo* toxicity tests revealed that the urea Schiff base complexes were harmless. There was no mortality, and all of the rats survived the treatment term. Overall, the results show that five urea Schiff base complexes, including cobalt, manganese, zinc, chrome, and copper, can be effective and prospective chemotherapeutic medicines for the ovarian cancer cell SKOV 3, with the copper-urea Schiff base complex being the most promising.

Funding: The authors gratefully acknowledge Qassim University, represented by the Deanship of Scientific Research, on the financial support for this research under the number (10190-cos-2020-1-3-I) during the academic year 1442 AH / 2020 CE.

Declaration of Competing Interest

The authors declare that they have no known competing financial interests or personal relationships that could have appeared to influence the work reported in this paper.

Acknowledgements

The authors gratefully acknowledge Qassim University, represented by the Deanship of Scientific Research, on the financial support for this research under the number (10190-cos-2020-1-3-I) during the academic year 1442 AH / 2020 AD.

References

Abdullahi, M., Uzairu, A., Shallangwa, G.A., Mamza, P., Arthur, D. E., Ibrahim, M.T., 2020. In-silico modelling studies on some C14-urea-tetrandrine derivatives as potent anti-cancer agents against prostate (PC3) cell line. J. King Saud Univ. Sci. 32, 770–779.

Adwin Jose, P. et al, 2020. Sankarganesh M.3 & Dhaveethu Raja J.4 & Sukkur Saleem S.1 Pyrimidine Derivative Schiff Base Ligand Stabilized Copper and Nickel Nanoparticles by Two Step Phase Transfer Method; in Vitro Anticancer, Antioxidant, Anti-microbial and DNA Interactions. J. Fluoresc. 30, 471–482.

Ahamad, M.N., Iman, K., Raza, M.K., Kumar, M., Ansari, A., Ahmad, M., Shahid, M., 2020. Anticancer properties, apoptosis and catecholase mimic activities of dinuclear cobalt (II) and copper (II) Schiff base complexes. Bioorg. Chem. 95, 103561.

Ahmed, M.F., Almalki, A.H., 2021. Design, synthesis, antiproliferative activity, and cell cycle analysis of new thiosemicarbazone derivatives targeting ribonucleotide reductase. Arab. J. Chem. 14, 102989.

Alam, M.M., Nazreen, S., Almalki, A.S.A., Elhenawy, A.A., Alsenani, N.I., Elbehairi, S.E.I., Malebari, A.M., Alfaifi, M.Y., Alsharif, M. A., Alfaifi, S.Y.M., 2021. Naproxen Based 1, 3, 4-Oxadiazole Derivatives as EGFR Inhibitors: Design. Synthesis, Anticancer, and Computational StudiesPharmaceuticals 14, 870.

Al-Hakimi, A.N., Shakdofa, M.M.E., El-Seidy, A.M.A., El-Tabl, A. S., 2011. Synthesis, Spectroscopic, and Biological Studies of Chromium(III), Manganese(II), Iron(III), Cobalt(II), Nickel(II), Copper(II), Ruthenium(III), and Zirconyl(II) Complexes of N1, N2 -Bis(3-((3-hydroxynaphthalen-2-yl)methylene-amino)propyl)phthalamide. J. Korean Chem. Soc. 55, 418–429.

Al-Hakimi, A.N., Alminderej, F., Aroua, L., Alhag, S.K., Alfaifi, M. Y., Mahyoub, J.A., Elbehairi, S.E., Alnafisah, A.S., 2020. Design, synthesis, characterization of zirconium (IV), cadmium (II) and iron (III) complexes derived from Schiff base 2-aminomethylbenzimidazole, 2-hydroxynaphtadehyde and evaluation of their biological activity. Arab. J. Chem. 13, 7378–7389.

Al-Hakimi, A.N., 2020. Synthesis, Characterization and Microbicides Activities of N-(hydroxy-4-((4-nitrophenyl) diazenyl) benzylidene)-2-(phenylamino) Acetohydrazide Metal Complexes. Egypt. J. of Chem. 63, 1509–1525.

Al-Hakimi, A.N., Shakdofa, M.M., Saeed, S., Shakdofa, A.M., Al-Fakeh, M.S., Abdu, A.M., Alhagri, I.A., 2021. Transition Metal Complexes Derived from 2-hydroxy-4-(p-tolyldiazenyl) benzylidene)-2-(p-tolylamino) acetohydrazide Synthesis, Structural Characterization, and Biological Activities. J. Korean Chem. Soc. 65 (2), 93–105.

Ali, I., Mahmood, L.M., Mehdar, Y.T., Aboul-Enein, H.Y., Said, M. A., 2020. Synthesis, characterization, simulation, DNA binding and anticancer activities of Co (II), Cu (II), Ni (II) and Zn (II) complexes of a Schiff base containing o-hydroxyl group nitrogen ligand. Inorg. Chem. Commun. 118, 108004.

Alminderej, F.M., Aroua, L., 2021. Design, Synthesis, Characterization and Anticancer Evaluation of Novel Mixed Complexes Derived from 2-(1H-Benzimizadol-2-yl) aniline Schiff base and 2-Mercaptobenzimidazole or 2-Aminobenzothiazole. Egypt. J. Chem. 64, 3–4.

Alorini, T.A., Al-Hakimi, A.N., Saeed, S.E.S., Alhamzi, E.H.L., Albadri, A.E., 2022. Synthesis, characterization, and anticancer activity of some metal complexes with a new Schiff base ligand. Arab. J. Chem. 15, 103559.

Andiappan, K., Sanmugam, A., Deivanayagam, E., Karuppasamy, K., Kim, H.S., Vikraman, D., 2018. In vitro cytotoxicity activity of novel Schiff base ligand–lanthanide complexes. Sci. rep. 8, 1–12.

Aras, B., Yerlikaya, A., 2016. Bortezomib and etoposide combinations exert synergistic effects on the human prostate cancer cell line PC-3. Oncology lett. 11 (5), 3179–3184.

Aroua, L., 2020a. Synthesis and characterization of novel mixed complexes derived from 2-aminomethylbenzimidazole and 2-(1*H*-Benzimidazol-2-yl) aniline and theoretical prediction of toxicity. Egypt. J. Chem. 63, 4757–4767.

Aroua, L.M., 2020b. Novel Mixed Complexes Derived from Benzoimidazolphenylethanamine and 4-(Benzoimidazol-2-yl) aniline: Synthesis, characterization, antibacterial evaluation and theoretical prediction of toxicity. Asian J. Chem 32, 1266–1272.

Asghar, F., Badshah, A., Lal, B., Zubair, S., Fatima, S., Butler, I.S., 2017. Facile synthesis of fluoro, methoxy, and methyl substituted ferrocene-based urea complexes as potential therapeutic agents. Bioorg. Chem. 72, 215–227.

Banti, C.N., Poyraz, M., Sainis, I., Sari, M., Rossos, G., Kourkoumelis, N., Hadjikakou, S.K., 2020. The periodic table of urea derivative: small molecules of zinc (II) and nickel (II) of diverse antimicrobial and antiproliferative applications. Mol. Diver. 24 (1), 31–43.

Bhuvaneswari, S., Umadevi, M., Vanajothi, R., 2020. Effects on anti-inflammatory, DNA binding and molecular docking properties of 2-chloroquinolin-3-yl-methylene-pyridine/pyrazole derivatives and

their palladium (II) complexes. Bioorg. Med. Chem. Lett. 30, 127593.
Buldurun, K., Tanış, E., Turan, N., Çolak, N., Çankaya, N., 2021a. Solvent effects on the electronic and optical properties of Ni (II), Zn (II), and Fe (II) complexes of a Schiff base derived from 5-bromo-2-hydroxybenzaldehyde. J. Chem. Res 45, 753–759.
Buldurun, K., Turan, N., Bursal, E., Aras, A., Mantarcı, A., Çolak, N., Gülçin, İ., 2021b. Synthesis, characterization, powder X-ray diffraction analysis, thermal stability, antioxidant properties and enzyme inhibitions of M (II)-Schiff base ligand complexes. J. Biomol. Struct. Dyn. 39 (17), 6480–6487.
Borriello, A., Caldarelli, I., Bencivenga, D., Stampone, E., Perrotta, S., Oliva, A., Della Ragione, F., 2017. Tyrosine kinase inhibitors and mesenchymal stromal cells: Effects on self-renewal, commitment and functions. Oncotarget 8, 5540.
Bose, S., Allen, A.E., Locasale, J.W., 2020. The molecular link from diet to cancer cell metabolism. Mol. Cell 78, 1034–1044. https://doi.org/10.1016/j.molcel.2020.05.018.
Crosbie, E.J., Einstein, M.H., Franceschi, S., Kitchener, H.C., 2013. Human papillomavirus and cervical cancer. The Lancet 382, 889–899.
Chandra, S., Kumar, S., 2015. Synthesis, spectroscopic, anticancer, antibacterial and antifungal studies of Ni (II) and Cu (II) complexes with hydrazine carboxamide, 2-[3-methyl-2-thienyl methylene]. Spectrochim. Acta A Mol. Biomol. Spectrosc. 135, 356–363.
Chaudhry, P., Asselin, E., 2009. Resistance to chemotherapy and hormone therapy in endometrial cancer. Endocr. Relat. Cancer 16 (2), 363–380.
Chen, S., Liu, X., Ge, X., Wang, Q., Xie, Y., Hao, Y., Zhang, Y., Zhang, L., Shang, w., Liu, Z. 2020. Lysosome-targeted iridium (III) compounds with pyridine-triphenylamine Schiff base ligands: syntheses, antitumor applications and mechanisms. Inorg. Chem. Front., 7, 91-100.
Cherukumalli, P.K.R., Tadiboina, B.R., Gulipalli, K.C., Bodige, S., Badavath, V.N., Sridhar, G., Gangarapu, K., 2022. Design and synthesis of novel urea derivatives of pyrimidine-pyrazoles as anticancer agents. J. Mol. Struct. 1251, 131937.
Crans, D.C., Koehn, J.T., Petry, S.M., Glover, C.M., Wijetunga, A., Kaur, R., Levina, A., Lay, P.A., 2019. Hydrophobicity may enhance membrane affinity and anti-cancer effects of Schiff base vanadium (V) catecholate complexes. Dalton Trans. 48, 6383–6395.
Das, M., Mukherjee, S., Koley, B., Choudhuri, I., Bhattacharyya, N., Roy, P., Samanta, B.C., Barai, M., Maity, T., 2020. Developing novel zinc (ii) and copper (ii) Schiff base complexes: combined experimental and theoretical investigation on their DNA/protein binding efficacy and anticancer activity. New J. Chem. 44, 18347–18361.
Dasgupta, S., Karim, S., Banerjee, S., Saha, M., Saha, K.D., Das, D., 2020. Designing of novel zinc (II) Schiff base complexes having acyl ydrazine linkage: study of phosphatase and anti-cancer activities. Dalton Trans. 49, 1232–1240.
Di, J., Rutherford, S., Chu, C., 2015. Review of the cervical cancer burden and population-based cervical cancer screening in China. Asian Pac. J. Cancer Prev. 16, 7401–7407.
Faidallah, H.M., Khan, K.A., Asiri, A.M., 2011. Synthesis and biological evaluation of new 3-trifluoromethylpyrazolesulfonyl-urea and thiourea derivatives as antidiabetic and antimicrobial agents. J. Fluorine Chem. 132, 131–137.
El-Saied, F.A., Salem, T.A., Shakdofa, M.M., Al-Hakimi, A.N., 2018. Anti-neurotoxic evaluation of synthetic and characterized metal complexes of thiosemicarbazone derivatives. Appl. Organomet. Chem. 32, 4215.
El-saied, F.A., Shakdofa, M.M.E., Al-Hakimi, A.N., Shakdofa, A.M.E., 2020. Transition metal complexes derived from*N*′-(4-fluorobenzylidene)-2-(quinolin-2-yloxy) acetohydrazide: Synthesis, structural characterization, and biocidal evaluation. Appl. Organomet Chem. 34, 5898.
El-Tabl, A.S., Shakdofa, M.M., Labib, A.A., Al-Hakimi, A.N., 2012. Antimicrobial activities of the metal complexes of N′-(5-(4-chlorophenyl) diazenyl)-2-hydroxybenzylidene)-2-hydroxybenzohydrazide. Main Group Chemi. 11 (4), 311–327.
Fayed, E.A., Eldin, R.R.E., Mehany, A.B., Bayoumi, A.H., Ammar, Y.A., 2021. Isatin-Schiff's base and chalcone hybrids as chemically apoptotic inducers and EGFR inhibitors; design, synthesis, antiproliferative activities and in silico evaluation. J. Mol. Struct. 1234, 130159.
Galil, M.S.A., Al-Hakimi, A.N., Alshwafy, R., AL OKAB, R.A., 2015. SYNTHESIS, CHARACTERIZATION AND ANTIFUNGAL, ANTIBACTERIAL STUDIES OF HYDRAZONE-OXIME METAL COMPLEXES. Journal of Applied Chemical Science. International, 9–20.
Garza-Ortiz, A., Maheswari, P.U., Siegler, M., Spek, A.L., Reedijk, J., 2013. A new family of Ru (II) complexes with a tridentate pyridine Schiff-base ligand and bidentate co-ligands: Synthesis, characterization, structure and in vitro cytotoxicity studies. New J. Chem. 37, 3450–3460.
Ghrab, S., Aroua, L., Beji, M., 2017a. A Facile and Efficient One-pot Three Component Route to New Bis (1, 2, 4-Oxadiazole) Linked with Polyoxyethylene Chain. Lett. Org. Chem. 14, 278–282.
Ghrab, S., Lahbib, K., Aroua, L., Beji, M., 2017b. Evaluation of antioxidant activity of selected new synthesized oxazolidin-2-one derivatives. J. Tunisian Chem. Soc. 19, 368–374.
Ghfar, A.A., El-Metwally, M.M., Shaaban, M., Gabr, S.A., Gabr, N. S., Diab, M.S.M., Aqel, A., Habila, M.A., Al-Qahtani, W.H., Alfaifi, M.Y., Elbehairi, S.E.I., AlJumah, B.A., 2021. Production of Terretonin N and Butyrolactone I by Thermophilic Aspergillus terreus TM8 Promoted Apoptosis and Cell Death in Human Prostate and Ovarian Cancer Cells. Molecules 26, 2816.
Gou, Y., Li, J., Fan, B., Xu, B., Zhou, M., Yang, F., 2017. Structure and biological properties of mixed-ligand Cu (II) Schiff base complexes as potential anticancer agents. Eur. J. Med. Chem. 134, 207–217.
Hanusova, V., Skalova, L., Kralova, V., Matouskova, P., 2015. Potential anti-cancer drugs commonly used for other indications. Curr. Cancer Drug Tar. 15, 35–52. https://doi.org/10.2174/1568009615666141229152812.
Hernández-Romero, D., Rosete-Luna, S., López-Monteon, A., Chávez-Piña, A., Pérez-Hernández, N., Marroquín-Flores, J., Colorado-Peralta, R., 2021. First-row transition metal compounds containing benzimidazole ligands: An overview of their anticancer and antitumor activity. Coord. Chem. Rev. 439, 213930.
Ismail, B. A., Nassar, D. A., Abd El–Wahab, Z. H., Ali, O. A., 2021. Synthesis, characterization, thermal, DFT computational studies and anticancer activity of furfural-type ydraz base complexes. J. Mol. Struct., 1227, 129393.
Jakob, C.H., Muñoz, A.W., Schlagintweit, J.F., Weiß, V., Reich, R. M., Sieber, S.A., Correia, J.D.G., Kühn, F.E., 2021. Anticancer and antibacterial properties of trinuclear Cu (I), Ag (I) and Au (I) macrocyclic NHC/urea complexes. J. Organomet Chem. 932, 121643.
Joshi, R., Kumari, A., Singh, K., Mishra, H., Pokharia, S., 2020. Triorganotin (IV) complexes of Schiff base derived from 1, 2, 4-triazole moiety: Synthesis, spectroscopic investigation, DFT studies, antifungal activity and molecular docking studies. J. Mol. Struct. 1206, 127639.
Kollu, U., Avula, V.K.R., Vallela, S., Pasupuleti, V.R., Zyryanov, G. V., Neelam, Y.S., Chamarthi, N.R., 2021. Synthesis, antioxidant activity and bioinformatics studies of L-3-hydroxytyrosine ydrazin N-alkyl/aryl substituted urea/thioureas. Bioorg. Chem. 111, 104837.
Lee, N., Spears, M.E., Carlisle, A.E., Kim, D., 2020. Endogenous toxic metabolites and implications in cancer therapy, Oncogene,39, 5709–5720, https://doi.org/10.1038/s41388-020-01395-9.

Li, J., Sasaki, H., Sheng, Y.L., Schneiderman, D., Xiao, C.W., Kotsuji, F., Tsang, B.K., 2000. Apoptosis and chemoresistance in human ovarian cancer: is Xiap a determinant? Neurosignals 9 (2), 122–130.

Lin, Y., Betts, H., Keller, S., Cariou, K., Gasser, G., 2021. Recent developments of metal-based compounds against fungal pathogens. Chem. Soc. Rev. 50, 10346.

Liu, C., Liu, X., Ge, X., Wang, Q., Zhang, L., Shang, W., Zhang, Y., Yuan, X.A., Tian, L., Liu, Z., You, J., 2020. Fluorescent iridium (III) coumarin-salicylaldehyde Schiff base compounds as lysosome-targeted antitumor agents. Dalton Trans. 49, 5988–5998.

Ma, Z.Y., Qiao, X., Xie, C.Z., Shao, J., Xu, J.Y., Qiang, Z.Y., Lou, J. S., 2012. Activities of a novel Schiff Base copper (II) complex on growth inhibition and apoptosis induction toward MCF-7 human breast cancer cells via mitochondrial pathway. J. Inorganic Biochem. 117, 1–9.

Madani, S., Mokhnache, K., Rouane, A., Charef, N., 2020. Synthesis, Characterization and In vitro evaluation of antibacterial and antifungal activities of New Schiff Base and Its Metal Complexes. Mater. Biomater. Sci 3, 001–009.

Matela, G., 2020. Schiff bases and complexes: a review on anti-cancer activity. Current Med. Chem.-Anticancer Agents 20, 1908–1917.

Martínez-Jiménez, F., Muiños, F., Sentís, I., Deu-Pons, J., Reyes-Salazar, I., Arnedo-Pac, C., Mularoni, L., Pinch, O., Bonet, J., Kranas, H., González-Pérez, A., López-Bigas, N., 2020. A compendium of mutational cancer driver genes. Nat. Rev. Cancer 20, 555–572. https://doi.org/10.1038/s41568-020-0290-x.

Miloud, M.M., El-ajaily, M.M., Al-noor, T.H., Al-barki, N.S., 2020. Antifungal Activity of Some Mixed Ligand Complexes Incorporating Schiff Bases. J. Bacteriol. Mycol. 7, 1122.

Mihanfar, A., Fattahi, A., Nejabati, H.R., 2017. MicroRNA-mediated drug resistance in ovarian cancer. J. Cell. Physiol. 234 (4), 3180–3191.

Mohapatra, R.K., El-ajaily, M.M., Alassbaly, F.S., Sarangi, A.K., Das, D., Maihub, A.A., Ben-Gweirif, S.F., Mahal, A., Suleiman, M., Perekhoda, L., Azam, M., Al-Noor, T.H., 2021. DFT, anticancer, antioxidant and molecular docking investigations of some ternary Ni (II) complexes with 2-[I-[4-(dimethylamino) phenyl] methyleneamino] phenol. Chem. Pap. 75, 1005–1019.

Nagalakshmamma, V., Venkataswamy, M., Pasala, C., Maheswari, A. U., Raju, K.T., Nagaraju, C., Chalapathi, P.V., 2021. A study on MAPK/ERK and CDK2-Cyclin-E signal switch "on and off" in cell proliferation by bis urea derivatives of 1, 4-Diisocyanatobenzene. Bioorg. Chem. 112, 104940.

Nicholson, K.M., Phillips, R.M., Shnyder, S.D., Bibby, M.C., 2002. In vitro and in vivo activity of LS 4477 and LS 4559, novel analogues of the tubulin binder estramustine. Eur. J. Cancer 38, 194–204.

OECD, 2001. OECD guideline for testing of chemicals 425; Acute Oral Toxicity – Up-and-Down Procedure.

Pal, R., Kumar, V., Gupta, A.K., Beniwal, V., 2014. Synthesis, characterization and DNA photocleavage study of a novel dehydroacetic acid based ydrazine Schiff's base and its metal complexes. Med. Chem. Res. 23, 3327–3335.

Parsekar, S.U., Paliwal, K., Haldar, P., Antharjanam, P.S., Kumar, M., 2022. Synthesis, Characterization, Crystal Structure, DNA and I Interactions, and Anticancer Activity of a Mononuclear Cu (II) Complex with a Schiff Base Ligand Containing a Thiadiazoline Moiety. ACS Omega 7, 2881–2896.

Parveen, S., 2020. Recent advances in anticancer ruthenium Schiff base complexes. Appl. Organomet. Chem. 34, 5687.

Poirier, D., Pahonţu, E., Fala, V., Gulea, A., Tapcov, V., Rosu, T., 2013. Synthesis and Characterization of Some New Cu (II). Antibacterial, Antifungal and in Vitro Antileukemia Activity, Ni (II) and Zn (II) Complexes with Salicylidene Thiosemicarbazones.

Poyraz, M., Sari, M., Banti, C.N., Hadjikakou, S.K., 2017. Synthesis, characterization and biological activities of copper (II) complex of 2-benzimidazolyl-urea and the nitrate salt of 2-benzimidazolyl-urea. J. Mol. Struct. 1146, 809–813.

Raoul, J.L., Kudo, M., Finn, R.S., Edeline, J., Reig, M., Galle, P.R., 2018. Systemic therapy for intermediate and advanced hepatocellular carcinoma: Sorafenib and beyond. Canc. Treat. Rev. 68, 16–24.

Ray, S., Mohan, R., Singh, J.K., Samantaray, M.K., Shaikh, M.M., Panda, D., Ghosh, P., 2007. Anticancer and antimicrobial metallopharmaceutical agents based on palladium, gold, and silver N-heterocyclic carbene complexes. J. Am. Chem. Soc. 129, 15042–15053.

Revathi, N., Sankarganesh, M., Dhaveethu Raja, J., Vinoth Kumar, G.G., Sakthivel, A., Rajasekaran, R., 2021. Bio-active mixed ligand Cu (II) and Zn (II) complexes of pyrimidine derivative Schiff base: DFT calculation, antimicrobial, antioxidant, DNA binding, anticancer and molecular docking studies. J. Biomol. Struct 39, 3012–3024.

Sabir, S., Yu, T.T., Kuppusamy, R., Almohaywi, B., Iskander, G., Das, T., Willcox, M.D.P., Black, D.S., Kumar, N., 2021. Novel seleno-and thio-urea containing dihydropyrrol-2-one analogues as antibacterial agents. Antibiotics 10, 321.

Shakdofa, M.M., Al-Hakimi, A.N., Elsaied, F.A., Alasbahi, S.O., Alkwlini, A.M.A., 2017. Synthesis, characterization and bioactivity Zn2+, Cu2+, Ni2+, Co2+, Mn2+, Fe3+, Ru3+, VO2+ and UO22+ complexes of 2-hydroxy-5-((4-nitrophenyl) diazenyl) benzylidene)-2-(p-tolyl-amino) acetohydrazide. Bull. Chem. Soc. Ethiop. 31, 75–91.

Shakdofa, M.M., Morsy, N.A., Rasras, A.J., Al-Hakimi, A.N., Shakdofa, A.M., 2021. Synthesis, characterization, and density functional theory studies of hydrazone–oxime ligand derived from 2, 4, 6-trichlorophenyl hydrazine and its metal complexes searching for new antimicrobial drugs. Appl. Organomet. Chem. 35, 6111.

Salgia, N.J., Zengin, Z.B., Pal, S.K., 2020. Tivozanib in renal cell carcinoma: A new approach to previously treated disease. Ther. Adv. Med. Oncol., 12

Saremi, K., Rad, S.K., Khalilzadeh, M., Hussaini, J., Majid, N.A., 2020. In vivo acute toxicity and anti-gastric evaluation of a novel dichloro Schiff base: Bax and HSP70 alteration. Acta Biochim. Biophys. Sin. 52, 26–37.

Savcı, A., Buldurun, K., Kırkpantur, G., 2021. A new Schiff base containing 5-FU and its metal Complexes: Synthesis, Characterization, and biological activities. Inorg. Chem. Commun. 134, 109060.

Savir, S., Wei, Z.J., Liew, J.W.K., Vythilingam, I., Lim, Y.A.L., Saad, H.M., Sim, K.S., Tan, K.W., 2020. Synthesis, cytotoxicity and antimalarial activities of thiosemicarbazones and their nickel (II) complexes. J. Mol. Struct. 1211, 128090.

Sedighipoor, M., Kianfar, A.H., Mohammadnezhad, G., Görls, H., Plass, W., Momtazi-Borojeni, A.A., Abdollahi, E., 2019. Synthesis, crystal structure of novel unsymmetrical heterocyclic Schiff base Ni (II)/V (IV) complexes: Investigation of DNA binding, protein binding and in vitro cytotoxic activity. Inorg. Chim. Acta 488, 182–194.

Sukanya, P., Venkata Ramana Reddy, C. 2018. Synthesis, characterization and in vitro anticancer, DNA binding and cleavage studies of Mn (II), Co (II), Ni (II) and Cu (II) complexes of Schiff base ligand 3-(2-(1-(1H-benzimidazol-2-yl) ethylidene) hydrazinyl) quinoxalin-2 (1*H*)-one and crystal structure of the ligand. Appl. Organomet. Chem., 32, 4526.

Sung, H., Ferlay, J., Siegel, R.L., Laversanne, M., Soerjomataram, I., Jemal, A., Bray, F., 2021. Global cancer statistics 2020: GLOBOCAN estimates of incidence and mortality worldwide for 36 cancers in 185 countries. CA Cancer J. Clin. 71, 209–249.

Sroor, F.M., Othman, A.M., Aboelenin, M.M., Mahrous, K.F., 2022. Anticancer and antimicrobial activities of new thiazolyl-urea derivatives: gene expression, DNA damage, DNA fragmentation and SAR studies. Med. Chem. Res. 31, 195–206.

Tabassum, S., Amir, S., Arjmand, F., Pettinari, C., Marchetti, F., Masciocchi, N., Lupidi, G., Pettinari, R., 2013. Mixed-ligand Cu (II)–vanillin Schiff base complexes; effect of coligands on their

DNA binding, DNA cleavage, SOD mimetic and anticancer activity. Eur. J. Med. Chem. 60, 216–232.
Tam, C., Rao, S., Waye, M.M.Y., Ng, T.B., Wang, C.C., 2021. Autophagy signals orchestrate chemoresistance of gynecological cancers. Biochim. Biophys. Acta (BBA)-Rev. Cancer 1875, (2) 188525.
Turan, N., Tanış, E., Buldurun, K., Colak, N., 2021. Synthesis, Structure, DFT Calculations, and In Silico Toxic Potential of Ni (II), Zn (II), and Fe (II) Complexes with a Tridentate Schiff Base. Russ. J. General Chem. 91 (8), 1572–1577.
Uprety, B., Chandran, R., Arderne, C., Abrahamse, H., 2022. Anticancer Activity of Urease Mimetic Cobalt (III) Complexes on A549-Lung Cancer Cells: Targeting the Acidic Microenvironment. Pharmaceutics 14, 211.
Vikram, V., Penumutchu, S.R., Vankayala, R., Thangudu, S., Amperayani, K.R., Parimi, U., 2020. Design, synthesis, molecular docking and cytotoxic activity of novel urea derivatives of 2-amino-3-carbomethoxythiophene. J. Chem. Sci. 132, 1–8.
Xie, X.X., Li, H., Wang, J., Mao, S., Xin, M.H., Lu, S.M., Mei, Q.B., Zhang, S.Q., 2015. Synthesis and anticancer effects evaluation of 1-alkyl-3-(6-(2-methoxy-3-sulfonylaminopyridin-5-yl) benzo [d] thiazol-2-yl) urea as anticancer agents with low toxicity. Bioorg. Med. Chem. 23, 6477–6485.
Xu, Y., Shi, Y., Lei, F., Dai, L., 2020. A novel and green cellulose-based Schiff base-Cu (II) complex and its excellent antibacterial activity. Carbohydr. Polym. 230, 115671.
Yadav, S., Narasimhan, B., kaur, H., 2016. Perspectives of benzimidazole derivatives as anticancer agents in the new era, Anti-Cancer Agent, Med. Chem. 16,1403–1425, https://doi.org/10.2174/18715206166661 51103113412.
Younes, N., Zayed, H., 2019. Genetic epidemiology of ovarian cancer in the 22 Arab countries: a systematic review. Gene 684, 154–164.
Zayed, E.M., Zayed, M.A., Fahim, A.M., El-Samahy, F.A., 2017. Synthesis of novel macrocyclic Schiff's-base and its complexes having N2O2 group of donor atoms. Characterization and anticancer screening are studied. Appl. Organomet. Chem. 31, 3694.
Zhang, Z., Li, J., Chen, H., Huang, J., Song, X., Tu, Z.C., Zhang, Z., Peng, L., Zhou, Y., Ding, K., 2022. Design, Synthesis, and Biological Evaluation of 2-Formyl Tetrahydronaphthyridine Urea Derivatives as New Selective Covalently Reversible FGFR4 Inhibitors. J. Med. Chem.
Ziegler, J., Schuerle, T., Pasierb, L., Kelly, C., Elamin, A., Cole, K.A., Wright, D.W., 2000. The propionate of heme binds N4O2 Schiff base antimalarial drug complexes. Inorg. Chem. 39, 3731–3733.

Further reading

World Cancer Research Fund. Available online: https://www.wcrf.org/dietandcancer/cancer-trends/prostate-cancer-statistics (accessed on 27 May 2021).
Wang, H., Xu, C., Zhang, X., Zhang, D., Jin, F., Fan, Y., 2020. Urease inhibition studies of six Ni (II), Co (II) and Cu (II) complexes with two sexidentate N2O4-donor bis-Schiff base ligands: An experimental and DFT computational study. J. Inorg. Biochem. 204, 110959.
Pahonţu, E., Proks, M., Shova, S., Lupaşcu, G., Ilieş, D.C., Bărbuceanu, .F., Socea, L.I., Badea, M., Păunescu, M., Istrati, D., Gulea, A., Drăgănescu, D., Pîrvu, C.E.D., 2019. Synthesis, characterization, molecular docking studies and in vitro screening of new metal complexes with Schiff base as antimicrobial and antiproliferative agents. Appl. Organomet. Chem. 33, 5185.
Shao, C., Wu, J., Han, S., Liu, Y., Su, Z., Zhu, H.L., Liu, H.K., Qian, Y., 2022. Biotinylated curcumin as a novel chemosensitizer enhances naphthalimide-induced autophagic cell death in breast cancer cells. Eur. J. Med. Chem. 228, 114029.